Coastal Engineering 192 (2024) 104541

Contents lists available at ScienceDirect

Coastal Engineering

journal homepage: www.elsevier.com/locate/coastaleng

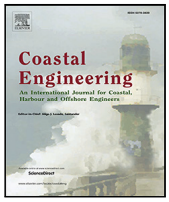

Influence of model configuration for coastal flooding across Europe

Marine Le Gal [a,b], Tomás Fernández-Montblanc [c,*], Juan Montes Perez [a,c], Enrico Duo [a,b], Paola Souto Ceccon [a,b], Paolo Ciavola [a,b], Clara Armaroli [d]

[a] Department of Physics and Earth Sciences, Università degli Studi di Ferrara, Via Saragat 1, Ferrara, 44122, Italy
[b] Consorzio Futuro in Ricerca, Via Giuseppe Saragat, 1, Ferrara, 44122, Italy
[c] Earth Sciences Department, University of Cadiz INMAR, Avda. República Saharaui s/n, Puerto Real, 11510, Spain
[d] Department of Biological, Geological and Environmental Sciences, University of Bologna Alma Mater Studiorum, via Zamboni 67, Bologna, 40126, Italy

ARTICLE INFO

Keywords:
Coastal flood
Numerical modelling
LISFLOOD-FP
Sensitivity analysis
Hydraulic parameters

ABSTRACT

Coastal flooding estimation at large scale, *e.g.* pan-European is usually performed using static method while dynamic method, in which numerical flood models are used to solve hydrodynamic equations, have proven to perform better. However, a numerical flood model can rapidly become computationally demanding. Thus, to respect the balance between efficiency and quality, models need to be properly configured. Usually, the model configuration is supported by calibration and validation. In the cases where it is not possible to appropriately implement calibration and validation through comparison against observed and measured data, sensitivity analyses can be applied in order to identify the key parameters that could influence the model capability to properly represent the modelled process. The present work aimed to identify influential model parameters across Europe and their relative importance in flood model configuration. Seventeen test cases were selected for which a LISFLOOD-FP model was developed, covering several sites across Europe and considering different storm events. A panoply of local morphologies and boundary conditions derived from the sites and storm event characteristics were used. For each test case, 72 simulations with different configurations were performed by varying the grid resolution, the numerical solver, the bottom friction and the wave set-up formulation used to estimate the total water level as a boundary condition. Two sensitivity analyses were performed on the modelled maximum flooded areas and water volumes using One-Driver-At-a-Time and variance-based methods. By using a k-means clustering method, the results of these sensitivity analyses allowed us to identify patterns through the test cases related to the geographical region, providing important information for the configuration of flood models across Europe. Both sensitivity analysis methods led to similar results highlighting dominant relative influences from the floodplain solver on the Atlantic coasts and from the boundary conditions on the Mediterranean ones. In addition the grid resolution was found to have great effect on the North and Baltic seas, while globally the friction was shown to impact the model's results less. The test cases were clustered using a k-means method using as input both the sensitivity analysis results and morphological factors. Depending upon the inputs, two different sets of clusters were generated revealing a complex relationship between the influence of the model's parameters and the selected morphological indicators.

1. Introduction

European countries are exposed to different coastal risks and hazards that are expected to grow due to climate change, sea-level rise and an increase of extreme event frequency, along with the growth of coastal populations and exposed assets (Merkens et al., 2016; Calafat et al., 2022; Portner et al., 2022). Usually the estimation of coastal flood risk is done at a local scale, and only a few works have focused on a global estimation (Barnard et al., 2014; Hinkel et al., 2014; Mokrech et al., 2015; Forzieri et al., 2016; Muis et al., 2016; Vousdoukas et al., 2016). Most of global models only consider a static flood approach (*i.e.*, bathtub) which often performs poorly (Bates et al., 2005; Seenath et al., 2016; Vousdoukas et al., 2016; Gallien et al., 2018). Bates et al. (2005) compared the flood extents resulting from a static and dynamic method, using LISFLOOD-FP (Bates and De Roo, 2000), with observed data for two regional coastal flood historical events. In both cases the dynamic models outmatched the static models, which greatly over-predicted the flood, exposing the limitation of the static model usage in large scale applications. Similarly, Vousdoukas et al. (2016) compared four different modelling methods including static and dynamic (LISFLOOD-FP model) approaches. From a validation test on the historical Xynthia

* Corresponding author.
E-mail address: tomas.fernandez@uca.es (T. Fernández-Montblanc).

https://doi.org/10.1016/j.coastaleng.2024.104541
Received 30 January 2023; Received in revised form 3 May 2024; Accepted 17 May 2024
Available online 23 May 2024

storm event at La Faute-sur-Mer (2010) and an application at pan-EU scale, they showed that the static models over-estimated the flood while the dynamic model yielded reasonable results.

During the development of a dynamic flood model, decision making about input model parameters is an essential step, both concerning physical processes and numerical settings. Ideally, the most advanced model configurations are used to accurately predict the flood magnitude. However, some parameters are more computationally expensive, such as advanced model solvers (3D Navier–Stokes model, for instance) or fine grid resolutions. To balance quality and efficiency, decisions on the configuration of the flood model must be made targeting specific goals, and adapted with the characteristics of the case study. To support this configuration, calibrations can be performed to adjust numerical parameters by comparison to observed data, as done by Lewis et al. (2013) and Olbert et al. (2017) with the friction. In the case of flooding, flood maps derived by satellite images and local flood markers can provide valuable information but their availability may be scarce, especially at large scale. When it is not possible to implement a careful calibration, sensitivity analyses are usually employed to identify the key parameters and their influence. Knowing which parameters have significant effect on the results in comparison to others in the targeted regions will be beneficial during the calibration of the flood model. Thus, the computational cost of the key parameters best settings could be compensated by the use of less consuming options for secondary parameters.

Generally, sensitivity analyses are performed focusing on particular parameters or phenomena, such as the boundary conditions and the input water level data, the grid characteristics and Digital Elevation Model (DEM) or floodplain friction parametrisations. The sensitivity analysis' result depends on the method used (Alipour et al., 2022), the sampling range of input parameters and the considered model's variables (Saltelli et al., 2010; Wagener and Pianosi, 2019). The DEM resolution was proved to have a significant impact, especially for the static flooding method (van de Sande et al., 2012; Leon et al., 2014; Wolff et al., 2016). The influence of the boundary conditions has widely been evaluated: Lyddon et al. (2020) investigated the influence of integrating tide, surge and waves; Brown et al. (2007) and de Moel et al. (2012) included breaching of natural or artificial defences in their models while Toimil et al. (2023) investigated the role of erosion; and Grilli et al. (2020) looked at the influence of using a wave dispersion model to generate the input. All these studies converged into an understanding of the important influence exerted by these input parameters. Brown et al. (2007), Lewis et al. (2011) and Smith et al. (2011) studied both the impact of roughness and boundary conditions, considering sea level and wave forcing, and sea-defence failures: in all cases they estimated that the impact of the roughness was much less than that of the forcing conditions. A few sensitivity analyses have already been performed, especially using LISFLOOD-FP for fluvial and coastal flood events, see Hall et al. (2005), Savage et al. (2016), Seenath (2018), Kıyıcı (2019), Lyddon et al. (2020). Savage et al. (2016) used an advanced variance-based method, estimating the Sobol indexes, to study the impact of spatial parameters such as the Digital Elevation Model, the grid resolution and the friction parameters for a single fluvial flood event. The study showed great complexity in the sensitivity of the models to their parameters, with relative influences of the parameters varying over time and space.

The previous analyses were usually applied to a restricted number of sites and events, and the results may not be extrapolated to other locations where the site settings are different. Kalakan et al. (2016) performed a sensitivity analysis integrating morphological factors such as the beach slope for idealised beach profiles, connecting smaller floods with steeper slopes. While there is a demand for flood risk assessment at pan-EU scale (Paprotny et al., 2019), according to the authors' knowledge, no sensitivity analysis has ever been performed at global scale considering different coastal morphologies and their associated storm conditions, which typically have a regional variability. The present work aimed to identify the key model parameters across Europe and assessing their relative influence by performing a sensitivity analysis on coastal flood models using recent storm events that occurred along European coastlines. For each test case (*i.e.*, selected locations and storm events), the relative influences of the grid resolution, the bottom friction, the boundary condition and the numerical solver were analysed by developing multiple flood models with different configurations and applying two sensitivity analyses. A global framework was employed to identify a pattern connecting the relative influence of the parameters and geographical location. This information could support the prioritisation of parameters depending on the area of interest, thus improving the efficiency of the model configuration and calibration.

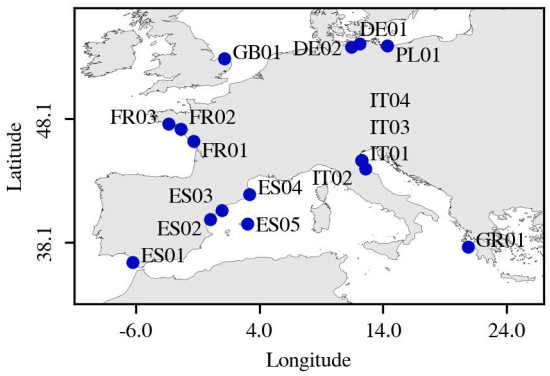

Fig. 1. Locations (blue dots) of the test cases that were selected for the sensitivity analyses.

2. Methods

2.1. Study areas and test cases

Seventeen test cases were selected from a database of extreme events on the European coast Souto Ceccon et al. (2022) developed by the Horizon 2020 ECFAS project (a proof-of-concept for the implementation of a European Copernicus coastal flood awareness system, https://www.ecfas.eu/) to be used for this sensitivity analysis. They are listed in Table 1 and can be localised on the map in Fig. 1. They represent a large variety of different coastal characteristics and oceanographic conditions (tidal range, storm surge level and wave energy) covering storms that occurred between 2010 and 2020 throughout Europe. This list gathers ten events covering fifteen sites, including multiple sites being hit by the same event and one site hit by multiple storms. Among the major events in the database, the test case FR01 represents the Xynthia storm that hit La Faute-Sur-Mer (France) in 2010. This event, characterised by a 100 year return period, had severe consequences with more than 40 casualties, over 500 km^2 of flooded land and damage estimated in excess of 2.5 billions euros, including windstorm damage, and about 1.25 billions only from the coastal flood (Vinet et al., 2012; Genovese and Przyluski, 2013; Kolen et al., 2013; Paprotny et al., 2018). In addition, four test cases were included (ES02 - ES05) representing the coastal flooding generated by the Gloria storm (2020) which was remarkable for its offshore intensity, breaking tide gauge records and causing severe consequences on the Spanish coast with flood reaching 3 km inland and a total economic loss combining marine, fluvial and rain damage estimated at 200 millions of euros (Pérez-Gómez et al., 2021). Coastal flood damage and compensation were estimated at 45 millions of euros for the regions of Catalonia, Balearic Islands, and Valencian Community (Luján López, 2022). On the other hand, two test cases were affected by the Axel storm in Germany (2017), in which little damage and flooding were reported (Souto Ceccon et al., 2022).

Table 1
List of the test cases extracted from the ECFAS database of extreme events (Souto Ceccon et al., 2022).

Test case ID	Event	Reference date	Site	Oceanographic region
FR01	Xynthia	27/02/2010	La Faute Sur Mer (FR)	Atlantic
FR02	No Name	02/01/2014	La Baule (FR)	Atlantic
FR03	No Name	02/01/2014	Lorient (FR)	Atlantic
GB01	Xaver	06/12/2013	Norfolk (GB)	North
IT01	Santa-Agatha	05/02/2015	Lido Delle Nazioni (IT)	Adriatic
IT02	Santa-Agatha	05/02/2015	Rimini (IT)	Adriatic
IT03	Vaia	29/10/2018	Lido Delle Nazioni (IT)	Adriatic
IT04	Detlef	11/11/2019	Lido Delle Nazioni (IT)	Adriatic
DE01	Axel	05/01/2017	Warnemunde (DE)	Baltic
DE02	Axel	05/01/2017	Wismar (DE)	Baltic
PL01	Axel	05/01/2017	Swinoujscie (PL)	Baltic
GR01	Ianos	18/09/2020	Laganas (GR)	Mediterranean
ES01	Emma	01/03/2018	Cadiz (ES)	Atlantic
ES02	Gloria	20/01/2020	Castellon (ES)	Mediterranean
ES03	Gloria	20/01/2020	Ebro (ES)	Mediterranean
ES04	Gloria	20/01/2020	Girona (ES)	Mediterranean
ES05	Gloria	20/01/2020	Mallorca (ES)	Mediterranean

Table 2
List of the Copernicus Marine Service ocean and wave models that were used in this work. The date of extraction indicates the months and year.

Copernicus Marine model	Date of extraction	References	List of associated test-cases
IBI_ MULTIYEAR	06-07 2021	Copernicus Marine Service (2020a), Copernicus Marine Service (2020b)	FR01, FR02, FR03, GB01, ES01
MEDSEA_ MULTIYEAR	06-10 2021	Escudier et al. (2020),Korres et al. (2021b)	IT01, IT02, IT03, IT04
BALTICSEA_ REANALYSIS	06 2021	Copernicus Marine Service (2018), Copernicus Marine Service (2020c)	DE01, DE02, PL01
MEDSEA_ ANALYSISFORECAST	09-11 2021	Clementi et al. (2021) Korres et al. (2021a)	GR01, ES02, ES03, ES04, ES05

2.2. Datasets

2.2.1. Digital elevation model

The topography was taken from the digital elevation model COP-EEA-DEM-10 which is part of the Copernicus DEM products (European Space Agency and Airbus, 2022). The latitudinal spatial resolution is $\sim$ 10 m with an absolute vertical accuracy lower than 4 m. The associated water body mask (European Space Agency and Airbus, 2022) was used to extract the coastal water extent, and thus to identify the coastline on which the boundary conditions for the flood model were imposed.

2.2.2. Land use and land cover data

To generate spatially varying friction maps, the friction parameter was derived from the European Environment Agency Land Use/Land Cover (EEA LU/LC) Coastal Zone layer 2018 (Innerbichler et al., 2021). The Coastal zone layer is composed by 71 environmental classes that were derived from Very High Resolution (VHR) satellite data and other available Earth Observation data. Its Minimum Mapping Unit (MMU) is 0.5 ha with a Minimum Mapping Width (MMW) of 10 m.

2.2.3. Water level

Total Water Levels (TWLs) in coastal areas can have different components produced either by atmospheric effects or oceanographic forcing. The TWL was produced by linear addition of the Sea Surface Height (SSH) component, resulting from the storm surge (e.g. induced by the wind or inverse barometer effect) and including the tide and the mean sea-level variability, and the wave set-up component. Coastal sea levels and wave bulk parameters required to estimate the wave set-up were extracted from the E.U. Copernicus Marine Service Information ocean products (https://resources.marine.copernicus.eu) which maintains up to date models (Irazoqui Apecechea et al., 2023). Table 2 gathers the Copernicus Marine models that were used for each test cases.

For both waves and SSH components, the hourly time series extracted from the closest point to the flood model ocean boundary were used to compute the TWL. The SSH of forecasts used in this work has been extensively validated in Irazoqui Apecechea et al. (2023). The different models that encompass the Copernicus Marine system showed overall a good performance in the reproduction of the extremes. Although they tend to underestimate the total water level showing centred RMSE of 0.29 cm and correlation values of 0.99 for TWL corresponding to percentile 95. When not included (i.e. Mediterranean sea), hourly time series of the tidal component was added from the FES2014 model (Lyard et al., 2021). The wave set-up component is derived from the hourly time series of significant wave height (Hs) and peak wave period (Tp) with spatial grid resolution of $\sim 2-5.5$ km.The validation of Copernicus Marine Service wave models showed a bias for the significant wave height varying between -6 and 2 cm (Copernicus Marine Service, 2017, 2020a; Korres et al., 2021b,a).

2.3. Numerical modelling method

The flood models were developed using the LISFLOOD-FP model (Bates and De Roo, 2000). The model grids are structured, homogeneous and cover 100 km alongshore length of the coastline with the domain centred on the area of interest. LISFLOOD-FP was configured to use the adaptive time step which means that the optimum time step to maintain model numerical stability is calculated by the solver and the initial time step is fixed at 10 s. The elevation was linearly interpolated from the DEM data (see Section 2.2.1) and the friction, when not uniform, was derived from LU/LC data (see Section 2.2.2) by associating a Manning coefficient to each LU/LC class using literature values (Chow, 1959; Papaioannou et al., 2018). The numerical floodplain solvers considered in the present work were the flow limited solver (Bates and De Roo, 2000) and the acceleration solver (Bates et al., 2010). The former consists of a uniform flow formula derived from the Manning equation, while the latter is a model based on the local inertia approximation that simplifies the shallow water wave formulation by neglecting the convective acceleration terms and is usually recommended for coastal modelling (Bates et al., 2010).

TWL time-series were imposed as boundary conditions at the coastline of the flood model. The time-series were directly interpolated from the ocean data (see Section 2.2.3) using a nearest point method. The TWL time-series were calculated by the linear addition of the SSH and the wave set-up. The modelling of wave nearshore propagation and swash excursion, in order to compute wave run-up values, requires accurate topo-bathymetric dataset to implement high resolution models. Given the European scale of the analysis, sufficiently detailed input datasets were not available. Therefore, in absence of high resolution

topo-bathymetric, information only wave setup contribution was considered, excluding swash processes. The parametrisation of wave set-up is a common practice (Dodet et al., 2019). Three parametrisations for the wave set-up (η_{wsu}) were considered in this work, derived from deep-water wave characteristics.

In the first parametrisation, the wave set-up is neglected ($\eta_{wsu} = 0$). The second option considers the generic semi-empirical formula of Stockdon et al. (2006) for which the wave set-up is approximated by:

$$\eta_{wsu} = 0.35 \times \tan\beta \sqrt{\frac{gT_p^2}{2\pi} \times Hs}, \quad (1)$$

where $\tan\beta$ is the foreshore slope and g the gravitational acceleration. To the authors' knowledge, a European database that gathers information on foreshore slope is not available. Athanasiou et al. (2019) gives worldwide estimations of coastal nearshore slope but with a resolution of 1 km. Thus, in the present case, an approximation of the foreshore slope computed as the average of the cross-shore slope, *i.e.* $\tan\beta$, was obtained from the DEM data through the following steps. First, slope grids were computed by applying the GDALDEM slope function on the DEM grid: the slope of one cell is calculated using the elevation of its 8 neighbours. Then, the first cell of the grid (that corresponds to the boundary position) was considered to be an approximation of the foreshore slope, hereinafter named gradient slope. This approximation showed limitations and bias, as a few unrealistic slopes were identified. A correct estimation of the foreshore slope would require a DEM with a high vertical and horizontal accuracy derived from, *e.g.*, direct field measurements or from the collection of precise remotely sensed data (*e.g.*, UAV and Lidar). To limit the impact of the identified biased slopes, that could result in unrealistic TWLs, only slope values inside beach polygons, *i.e.*, defined by the Coastal Zone LU/LC 2018 extension, were considered, and the slopes exceeding the standard deviation were replaced by the mean slope value computed as the average of the gradient slope inside the beach polygon. The third option considers the semi-empirical formulation derived by Holman and Sallenger (1985) and recommended by U.S. Army Corps of Engineers (2002):

$$\eta_{wsu} = 0.2 \times Hs. \quad (2)$$

The vertical DEM and SSH data are referenced to the 2008 and GOCE geoid models, respectively. To present the cross-referenced data, both datasets were adjusted to the Mean Sea Level (MSL). To do so, the data were corrected using Mean Dynamic Topography (MDT) models that are given by the average of the difference between the mean sea surface and the geoid models. The DEM was corrected using the 12 year MDT from Andersen and Knudsen (2009) also based on the 2008 geoid model, and the SSH data were corrected with the MDT taken from the corresponding Copernicus Marine Service ocean model.

2.4. Sensitivity analysis method

The sensitivity analysis was applied to the seventeen test cases described in Section 2.1. It was performed on four major parameters selected for their relevance to flood magnitude: the grid resolution (dx), the numerical floodplain solver (FS), the Manning friction coefficients (F) and the boundary condition with the wave set-up formulation (WS). The different options tested for each of these parameters are detailed in Table 3. A descriptive indicator was attributed to the different options: low-medium-high for numerical parameters and null-basic-advanced for formulation options. By testing the overall influence of multiple parameters, this approach allowed us to explore the relative computational costs and qualitative benefits of altering each parameter's options.

A flood model was developed for each combination of the four parameters for all the test cases, leading to a total of 1224 numerical models to carry out the as inputs for the sensitivity analyses. The modelling outputs used for performing the sensitivity analyses are both the Maximum Flood Areas (m^2, M.F.A.) and Maximum Water Volumes (m^3, M.W.V.), as the sum of the non-simultaneous maximum water depth per cell in the whole emerged domain (as defined by Fernández-Montblanc et al., 2020). The sensitivity analyses were performed with two methods: a One-Driver-At-a-Time (ODAT, Section 2.4.1) and variance based (Section 2.4.2) methods. A k-means clustering algorithm was applied to the sensitivity analysis results using the Euclidean distance between variables. The algorithm used in this work is that of Matlab v2021b based on Lloyd (1982). A convergence test was performed and only the final result is presented here.

2.4.1. One driver at a time method

With the One-Driver-At-a-Time method (ODAT), the variations in the output result Y (flood extent or volume of water) induced by the change of only one parameter x_i (dx, F, FS or WS) were evaluated using the standard deviation (std). The average of the variations per parameters was then estimated using the equation:

$$M_{xi} = \overline{std(Y|x_{j,k,l})}. \quad (3)$$

where $x_{i,j,k,l}$ correspond to the parameters listed in Table 3. A higher value of M_{xi} corresponds to a more influential parameter. In addition to the average variation, the standard deviation was estimated, being:

$$N_{xi} = std\left(std(Y|x_{j,k,l})\right). \quad (4)$$

N_{xi} gives a measure of the dependence of the variation in the values to the other parameters. A small N_{xi} corresponds to a consistent variation across the model's parameter option independently from the other parameter combinations, and thus it portrays a more robust representation of the impact of the parameter. A high N_{xi} suggests that the variation of the impact of the considered parameter depends on the combinations of the other parameter and could reveal a co-dependence among parameters.

2.4.2. Variance based method

The second method implemented was variance based. For each of the parameters, the first order Sobol index was estimated according to the definition by Saltelli et al. (2010) and to the usage by Savage et al. (2016):

$$S_{xi} = \frac{V_{xi}[E_{x\sim i}(Y|x_i)]}{V(Y)}, \quad (5)$$

where V_{xi} represents the variance induced by the factor x_i in the expected values E of Y while keeping x_i fixed. S_{xi} is an indicator of the relative influence in comparison with the other parameters with the highest value suggesting a stronger influence of the parameter on the others.

For both methods, the order of the values of the indicator gives the ranking of the parameters that can be compared across the test cases. However, the values of the indicator are specific of each test case and cannot be compared across them.

3. Results

3.1. General result

For the four parameters and each of the other parameter combinations, the relative evolution of the maximum flood areas (M.F.A.) and maximum water volumes (M.W.V.) were estimated by normalising the result with the outputs of the benchmark for all test cases. The lowest or basic option described in the first row of Table 3 was considered as the baseline. The box plot with the main statistics (median, 25th/75th percentiles, minimum/maximum) are shown in Fig. 2. The same trends are found for M.F.A. and M.W.V. Both M.F.A and M.W.V decrease along with the grid resolution (Fig. 2(a)) and increase with the advanced solver (Fig. 2(b)). Integrating the wave set-up in the TWL increases the water level, and thus leads to an increase of the volume of water

Table 3
The four parameters tested inside the LISFLOOD-FP models and their various options.

Mesh resolution (dx in m)	Floodplain solver (FS)	Manning coefficient (F in s $m^{-1/3}$)	Wave set-up formulation (WS)
Low: 100	Basic: Flow limited Bates and De Roo (2000)	Low: 0.0013	Null: No wave set-up
Medium: 50	Advanced: Acceleration Bates et al. (2010)	Medium: 0.025	Basic: $0.2 \times H_s$ as suggested by Holman and Sallenger (1985) and U.S. Army Corps of Engineers (2002)
High: 25	–	High: 0.05	Advanced: Generic formula from Stockdon et al. (2006)
–	–	Adapted: LU/LC derived	–

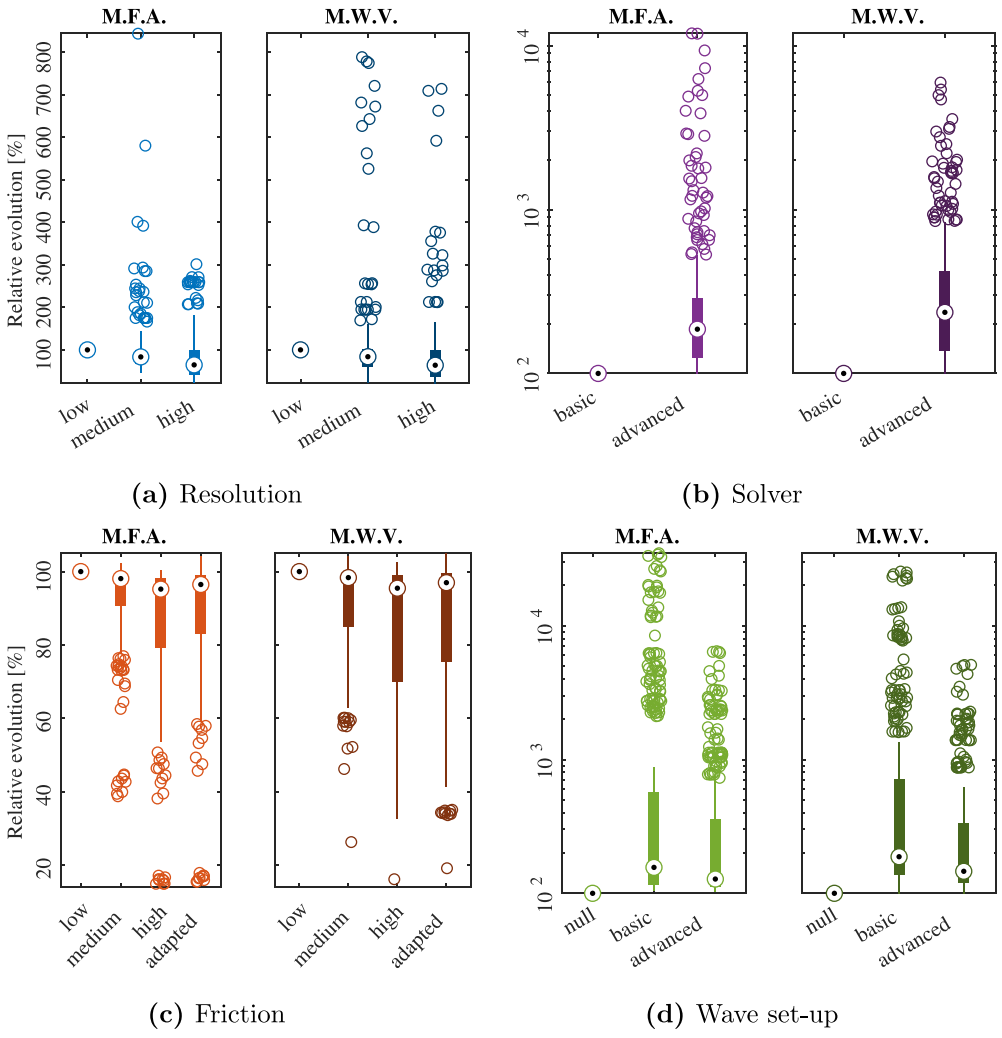

Fig. 2. Relative evolution of the Maximum Flood Area (M.F.A., left panel/light colour) and the Maximum Water Volume (M.W.V., right panel/dark colour) to the lowest or most basic option by considering all the combinations of parameters for the seventeen test cases. The black dot, thick line, thin line, single circles represent the median, 25th/75th percentiles, minimum/maximum and outliers.

flooding the coastal area. Between the two approximations of the wave set-up, the basic option leads to globally larger flood extents than with the advanced option (Fig. 2(b)). Finally, the outputs tend to decrease with the increase of the friction (from low to high, Fig. 2(c)). Using an adapted friction derived from the LU/LC characteristics reduces the flooding extent in comparison to the low/medium friction coefficients, but not as much as using the highest friction option.

Concerning the sensitivity analysis and the evaluation of the influence indicators (M_{xi} and S_{xi}), the global results and rankings are gathered in the maps of Fig. 3 for each test case. In Figs. 3, the marker size is proportional to M_{xi} and S_{xi}. Although slight differences can be observed between the flooded area and the water volume analysis, the ranking of the parameters remains globally equivalent; therefore only the results for the flooded area are discussed. With the variance based method, the differences between the parameter indicators are accentuated in comparison with those of the ODAT method, that could be related to the standard deviation and variance properties used to define the indicators. Indeed, the variance being the square of the standard deviation, its derivative will be bigger than the one of the standard deviation, as long as the latter is bigger than 0.5. The flooded area differences obtained in this study are larger than 0.5, which could explain why the variance based method better separates the results. The same patterns appear in both methods, giving consistent results and highlighting the robustness of the analysis. Detailed estimation

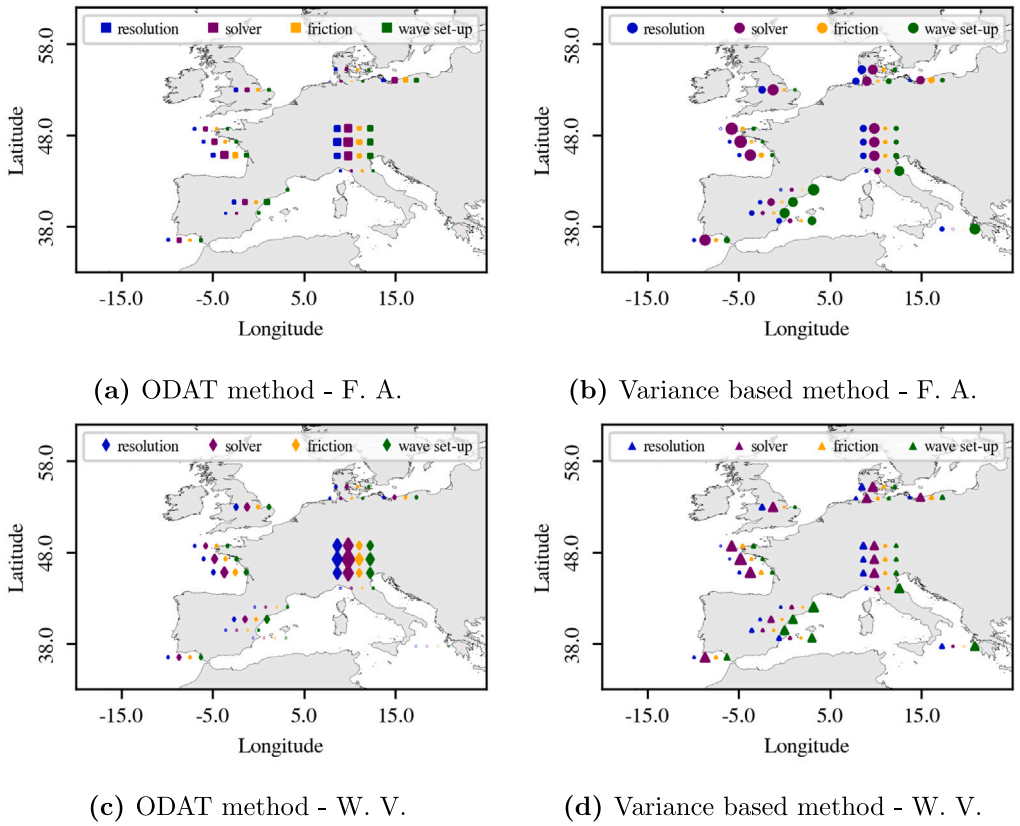

Fig. 3. Sensitivity analysis results for each test case using the ODAT (3(a) and 3(c)) and variance method (3(b) and 3(d)) on the Maximum Flooded Area, F.A., (3(a) and 3(b)) and the Maximum Water Volume, W. V., (3(c) and 3(d)). The marker size is proportional to M_{xi} and S_{xi}. The purple, orange, green and blue markers correspond to the solver, friction, boundary condition and resolution parameter results.

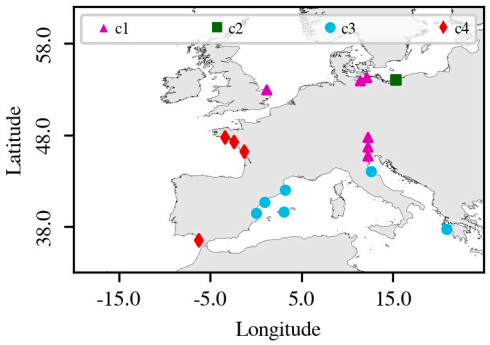

Fig. 4. Clusters identified by the k-means clustering method with the S.A. result as input.

of M_{xi} and S_{xi} for each test case can be found in Appendix (see Figs. A.15–A.16) for the Maximum flood extent output.

Out of the seventeen test cases, eleven cases are more influenced by the solver parameter while six cases are controlled by the boundary conditions. Although the solver parameter ranks first in all cases, in seven cases the boundary conditions have a significant impact on the results. With respect to the other parameters, friction does never show a relevant influence.

The sensitivity analysis leads to the identification of groups of test cases. A k-means clustering method was implemented to clearly identify such groups. An optimal number of four clusters was identified via a convergence test and was used as input for the k-means method. The clusters of test cases are visible in Fig. 4.

The two test cases DE01 and DE02 in the Baltic sea, the test case GB01 on the North sea affected by Xaver (2013) and the test cases in the northern part of the Adriatic (IT01, IT03, IT04) are grouped considering a dominant influence of the solver, and also, although less dominant, of the resolution (cluster 1 in Fig. 4). The test case PL01 at Swinoujscie is self clustered (cluster 2) with the solver being the most influencing parameter followed by the friction. All the test cases on the Mediterranean coast, except the northern cases of the Adriatic, are clustered together (cluster 3) with the boundary condition as the dominant parameter. Eventually, all the test cases on the Atlantic are grouped in the cluster 4 with a clear dominance of the solver. Each of these clusters are detailed below.

3.2. Results per cluster

3.2.1. Cluster 1 & 2: North and baltic seas and northern adriatic group

The North and Baltic Seas and Northern Adriatic group (GB01, DE01, DE02, IT01, IT03, IT04) show a lower dominance of one parameter over the others. While the influence of the solver parameter is still relevant, also the grid resolution drives significant variations on the flood extent. The associated flood maps are illustrated in Fig. 5. The differences between the flood models using various resolution mainly appear on the landward boundary of the flooded area, where the 100 m resolution cells cover a larger portion of the territory, compared to the 50 m resolution, while at 25 m the flooded area has the lower extension. In addition, with the highest resolution, some coastal areas are not flooded. The test case PL01 at Swijnouscie during the Axel storm (2017) does not group with other test cases and creates the cluster 2. This is the only test case showing a relative sensitivity to the friction parameter. The configuration with the lower values leads to the propagation of the flood water up to the lagoon situated in the

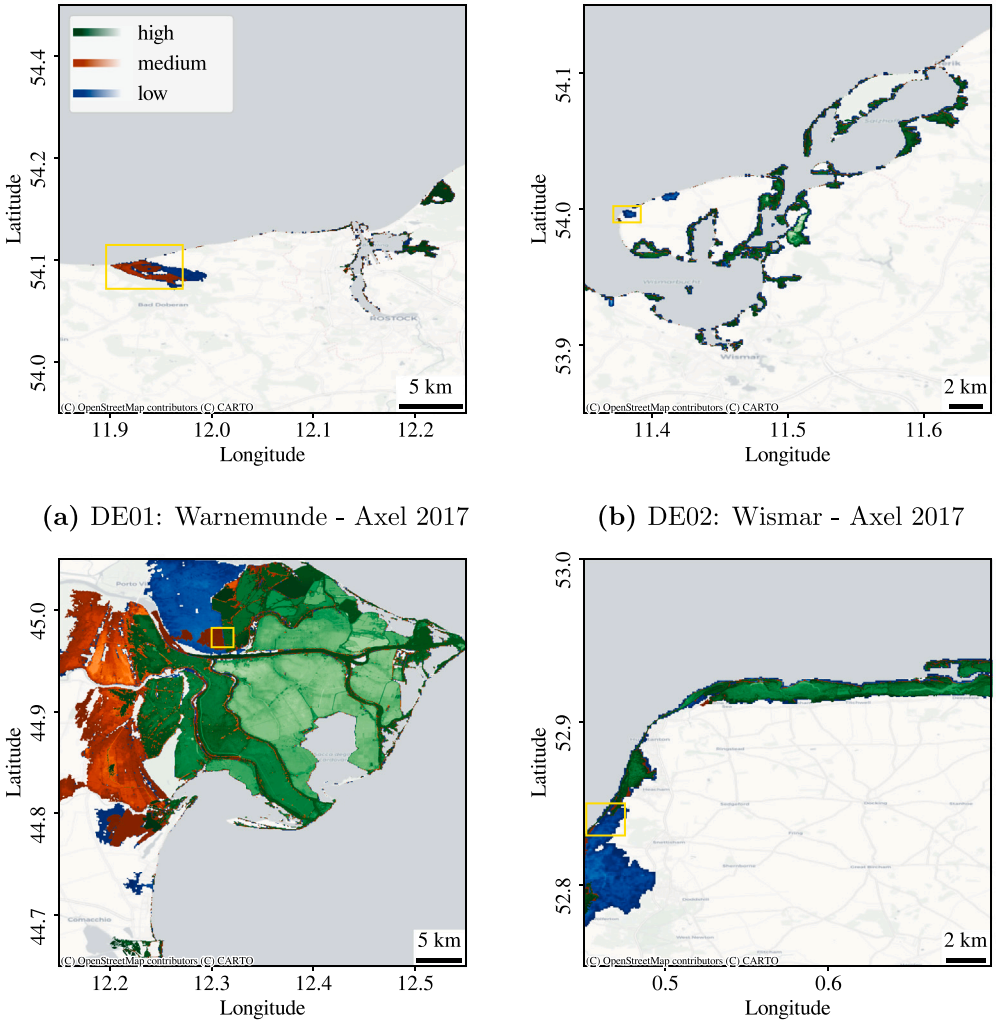

(a) DE01: Warnemunde - Axel 2017

(b) DE02: Wismar - Axel 2017

(c) IT03: Lido Delle Nazioni - Vaia 2018

(d) GB01: Norfolk - Xaver 2013

Fig. 5. Comparison of the flooded areas between the low (blue) - medium (red) - high (green) resolution for the North and Baltic seas and Northern Adriatic group test cases. The intensity of the colour from dark to light indicates an increase in flood water depth. The flood models correspond to the advanced solver, the adapted friction and the basic wave set-up option. The yellow boxes correspond to the zoom extent of the inset maps of Fig. 12. The background maps were generated using the OpenStreetMap database available through Python (Open Database License).

south of the modelling domain, while the water propagation stops on the land with the roughest friction and with the LU/LC derived friction (Fig. 6).

3.2.2. Cluster 3: Mediterranean group

The wave set-up formulation has a larger impact compared to the other three parameters for the test cases in the Mediterranean Sea, except at Lido Delle Nazioni. In Fig. 7, the flood extension for the model with null, basic and advanced options (see Table 3 for the corresponding formulation) are overlaid for ES02, ES03, ES04 and IT02. Globally, these test cases show little flooding, with the exception of ES03 that focuses on the Ebro delta. The boundary conditions that include the basic and advanced options generate larger flooding, while the site show relatively limited flooding using the model configuration that does not include the wave set-up (null option). In the latter configuration, the flooding is limited to the coastline, while it propagates further inland and inside river outlets with the advanced option, and even more with the basic option (ES02 and ES04). The flood in the Ebro Delta during the Gloria storm (ES03) was previously analysed and modelled by Amores et al. (2020). They developed a regional hydrodynamic model using SCHISM, fully coupled with the spectral wave model WWM-III, with a spatial resolution at the Ebro Delta of approximately 30 m. The study concluded that their simulation underestimated the flooding when compared to a flood map derived from a Sentinel-1 satellite image. This discrepancy was attributed to the absence of the precipitation contribution in their model. By qualitatively comparing the (Amores et al., 2020) flood map to the one of the present analysis displayed in Fig. 7(c), their simulation indicates a flood extension covering an area with an extension between the area derived from the modelling outputs of the configuration without wave set-up (green layer) and with an advanced wave set-up formulation (red layer). While comparing modelled to observed flood maps derived from satellite images is a complex exercise, as pointed out by Kiesel et al. (2023) and Le Gal et al. (2023) among others, both model outputs and satellite images show coherent flood maps. This also suggests a potential over-prediction of models that use the basic wave set-up formulation.

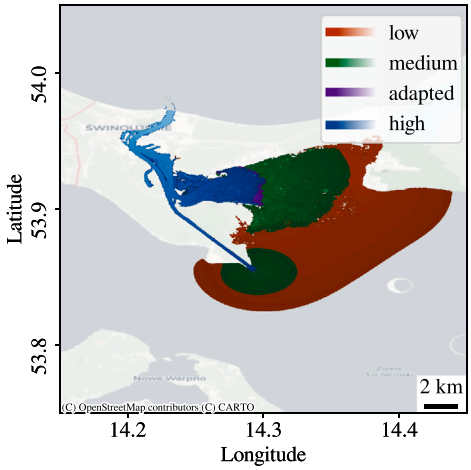

Fig. 6. Comparison of the flooded areas for the test case PL01 at Swijnouscie during the Axel storm (2017) between the low (red), medium (green), high (blue) and adapted (purple) friction options. The intensity of the colour from dark to light indicates an increase in flood water depth. The flood extension with the adapted option is similar to the one of the low option, and thus mainly covered in the map. The background maps were generated using the OpenStreetMap database available through Python (Open Database License).

3.2.3. Cluster 4: Atlantic group

The Atlantic coast test cases show a more significant sensitivity to the floodplain solver option. The flood maps for both options of solver regarding the test cases FR02, FR01, FR03 and ES01 are represented in Fig. 8. From a qualitative comparison, the acceleration solver (advanced option) propagates the flooding further in low-lying areas such as wetlands. The flooding during the Xynthia storm at La Faute-sur-Mer in 2010 (FR01) has been extensively studied and modelled by (Vousdoukas et al., 2016) for validation purpose and Bertin et al. (2014) among others. The latter employed the 2D hydrodynamic barotropic SELFE model, fully coupled with the spectral wave model WWM-II, with a spatial resolution of approximately 5 m at the coast. In comparison to Bertin et al. (2014) flood map and to the observed data used by the authors, it is evident that the present model with the basic solver configuration underestimates the flood extension. Meanwhile, the advanced solver model underestimates the flood extension towards the East and overestimates it towards the North of the Aiguillon Bay (North of La Rochelle), showing results consistent with the predicted flood map of the 100 m LISFLOOD-FP model of Vousdoukas et al. (2016). Such discrepancies highlight the limitations of the basic solver while the similarity between the present advanced solver and the results of Vousdoukas et al. (2016) compared to that of Bertin et al. (2014) reveals the influence of the modelling approach and of the spatial resolution.

3.3. Parameter co-dependence

In addition to the average variation M_{xi}, the standard deviation N_{xi} of the variation was calculated and is shown in Appendix. Histograms of the N_{xi} normalised by M_{xi} are shown on Fig. 9. For all parameters, normalised N_{xi} reach values above 100%, meaning that the influence of one parameter is largely dependent on the combination of the other parameters. This is particularly true for the friction parameter, which, using M_{xi}, is less significant than the other parameters, but shows a lot of differences in its influence. On the other hand, the impacts of the boundary condition and the estimation of the wave set-up are less variable and thus their influence is independent from the other chosen parameters.

4. Discussions

4.1. Boundary condition influence

The boundary condition is the most influencing parameter in the Mediterranean group, meaning that the flood models are sensitive to the inclusion of the wave set-up component. The wave set-up component is site and storm specific as described in Section 2.2.3. To relate the result of the sensitivity analyses with the wave set-up process, the relative contribution of the wave set-up to the total water level used to force the numerical model is estimated through the comparison of the maximum water depth (D) at the coastline computed with the basic and null configurations of the flood models (i.e., the two defined options that do not include or calculate the wave set-up) . As this difference is estimated at every coastline point, the average value is considered to be representative of the test case. The relative wave set-up contribution (wsu^*) is calculated as:

$$wsu^* = \overline{\frac{D_{WSbasic} - D_{WSnull}}{D_{WSbasic}}}, \tag{6}$$

and is shown in Fig. 10(a).

wsu^* reaches 100% for the Mediterranean test cases, while it is smaller on the Atlantic and North Sea sites (less than 50%), with a peak at 70% on the northern Adriatic sea. A wsu^* of 100% can be computed when the modelled water elevation without wave set-up contribution is below mean sea level, as illustrated in Fig. 10(b) for the test case ES02, leading to $D_{WSnull} = 0$. Therefore, positive water elevations are only computed when the wave set-up is accounted for, leading to flooding and non-null maximum water depths at the coastline. For the Gloria storm (2020), Amores et al. (2020) estimated the contribution of different hydrodynamic processes and components to the storm surge along the Mediterranean coastline of Spain using numerical models. The authors highlighted the importance of including the wave set-up component together with the use of a coupled hydrodynamic and spectral wave model. The observed discrepancies between the importance of the wave setup contribution showed in this study and in Amores et al. (2020) for the Gulf of Valencia can be explained by the overestimation of wave setup in the present study. In this case the wave direction does not transfer the total energy to the shore and it produces the overestimation of wave setup. Also the underestimation of significant wave height and period showed in Amores et al. (2020) could contribute to the differences observed. Additionally, the incorporation of the mean sea level variability, while neglected by Amores et al. (2020), shows minimum values during winter months in the Mediterranean sea (see Fernández-Montblanc et al., 2020; Criado-Aldeanueva et al., 2008; García-García et al., 2010), reduces the TWL and increases the relative contribution of wave setup. This explains the negative values of TWL with null wave setup contribution showed in Fig. 10b that are in agreement with the TWL values computed for the Gloria storm reported by Irazoqui Apecechea et al. (2023).

The geographical difference of the relative contribution of the wave set-up is a consequence of the wave and current dynamics of the Mediterranean Sea that can be defined as a micro-tidal basin which is generally not prone to surge development. Indeed, the wind component of the storm surge is inversely proportional to the water depth (Pugh, 1987; Fernández-Montblanc et al., 2019) and, thus, better develops in a shallow and wide continental shelf, such as in the North Sea, than in a steep and narrow continental shelf, like the Mediterranean (Toomey et al., 2022). Consequently, the relative contribution of the waves increases because the wind surge component contribution is reduced in the Mediterranean than in the Atlantic or North Sea, thus corroborating the present results. Melet et al. (2018) estimated the contribution of the tide, storm surge and wave components to extreme water level using data observed between 1993 and 2015 at global scale. The authors found a larger relative contribution of nearshore wave components (set-up plus swash) in the West Mediterranean sites than in the Atlantic

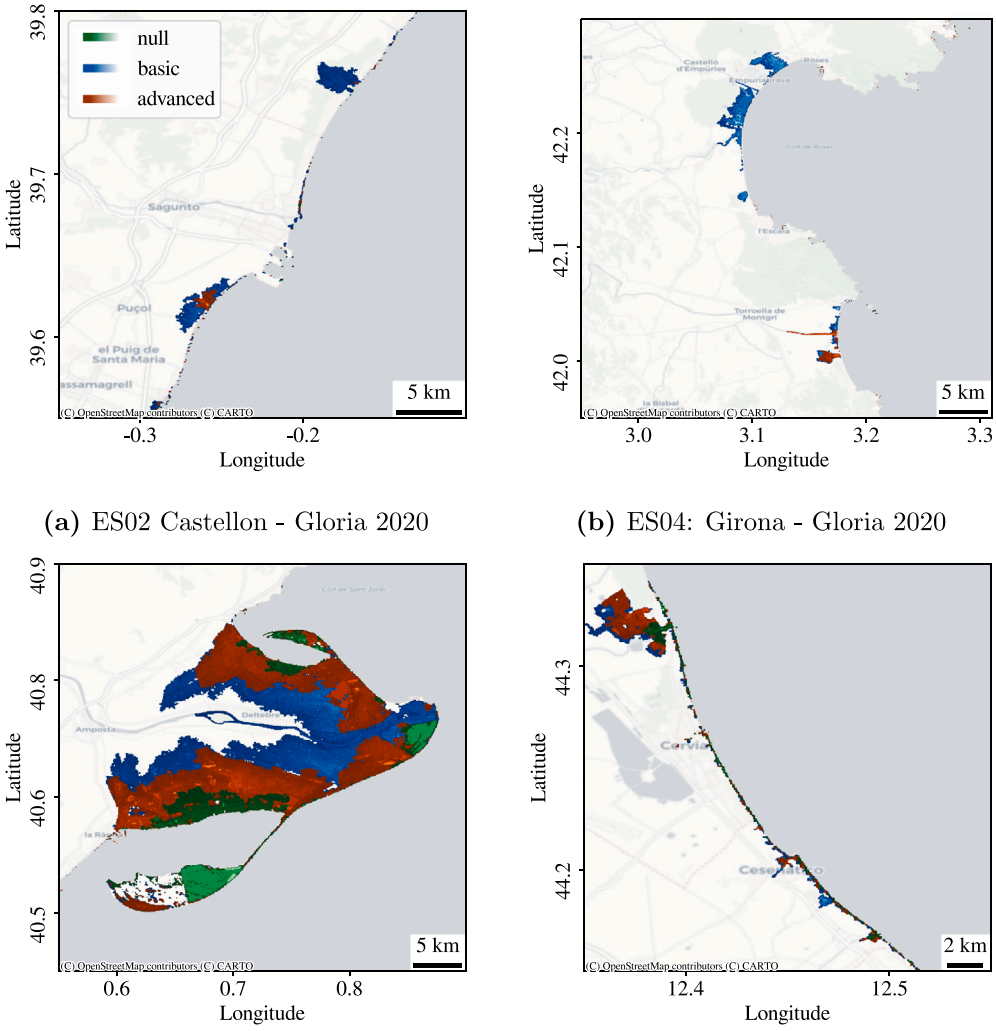

(a) ES02 Castellon - Gloria 2020

(b) ES04: Girona - Gloria 2020

(c) ES03: Ebro - Gloria 2020

(d) IT02: Rimini - Santa-Agatha 2015

Fig. 7. Comparison of the flood extension between the null (green layer), basic (blue layer) and advanced (red layer) wave set-up formulation for the Mediterranean group test cases. The intensity of the colour from dark to light indicates an increase in flood water depth. The flood models correspond to the medium resolution, the adapted friction and the advanced solver. The background maps were generated using the OpenStreetMap database available through Python (Open Database License).

and North Sea coasts. From a broader approach, the inclusion of the wave components in the estimation of the extreme total water level and its interaction with the other components have been widely discussed by Staneva et al. (2016), Melet et al. (2018), Idier et al. (2019), Marcos et al. (2019) among others. The literature highlights the importance of the inclusion of the wave components in the estimation of the total water level, either by using empirical formulation, as done in the present work, or by coupling wave and hydrodynamics models. The results of the present study underline the importance of the wave set-up in the Atlantic and North Sea and particularly show its priority contribution in Mediterranean regions.

4.2. Floodplain solver influence

The choice of the floodplain solver greatly influences the output results for most of the test cases and in particular those located on the Atlantic coast (Fig. 3). The acceleration solver propagates the inundation further inside embayments, estuaries and water bodies, because the acceleration solver integrates more wave propagation processes than the flow limited solver (Bates et al., 2013). This is also visible in the test cases from the North and Baltic Seas, Lido delle Nazioni, as well as the test case GB01 (Xaver storm, 2013) in Norfolk (North Sea) which is characterised by the presence of salt marshes. Using the LU/LC coastal zone 2018 layer, the flood prone areas for each test case is estimated by targeting the classes defined as wetland, beach, dune, and river bank, see Fig. 11. The Atlantic group plus the GB01 test case represents the largest flood-prone area that shows a correlation with the solver parameter. To go further, more developed numerical solvers of LISFLOOD-FP could be used, integrating the full shallow water system (Villanueva and Wright, 2006; Neal et al., 2012; Bates et al., 2013). However, the acceleration solver was shown to be relevant for coastal flooding by Neal et al. (2012) and Shaw et al. (2021). They reached this conclusion by comparing the results obtained with the acceleration solver with the ones generated by solvers based on the full shallow water equation at first and second degrees. This indicates the limitation of the flow limited solver (basic option)for coastal event modelling when river discharge is omitted. In the present work the influence of fluvial flooding is not investigated, but integrating the fluvial dynamic could impact the results (Kumbier et al., 2018; Bevacqua et al., 2020).

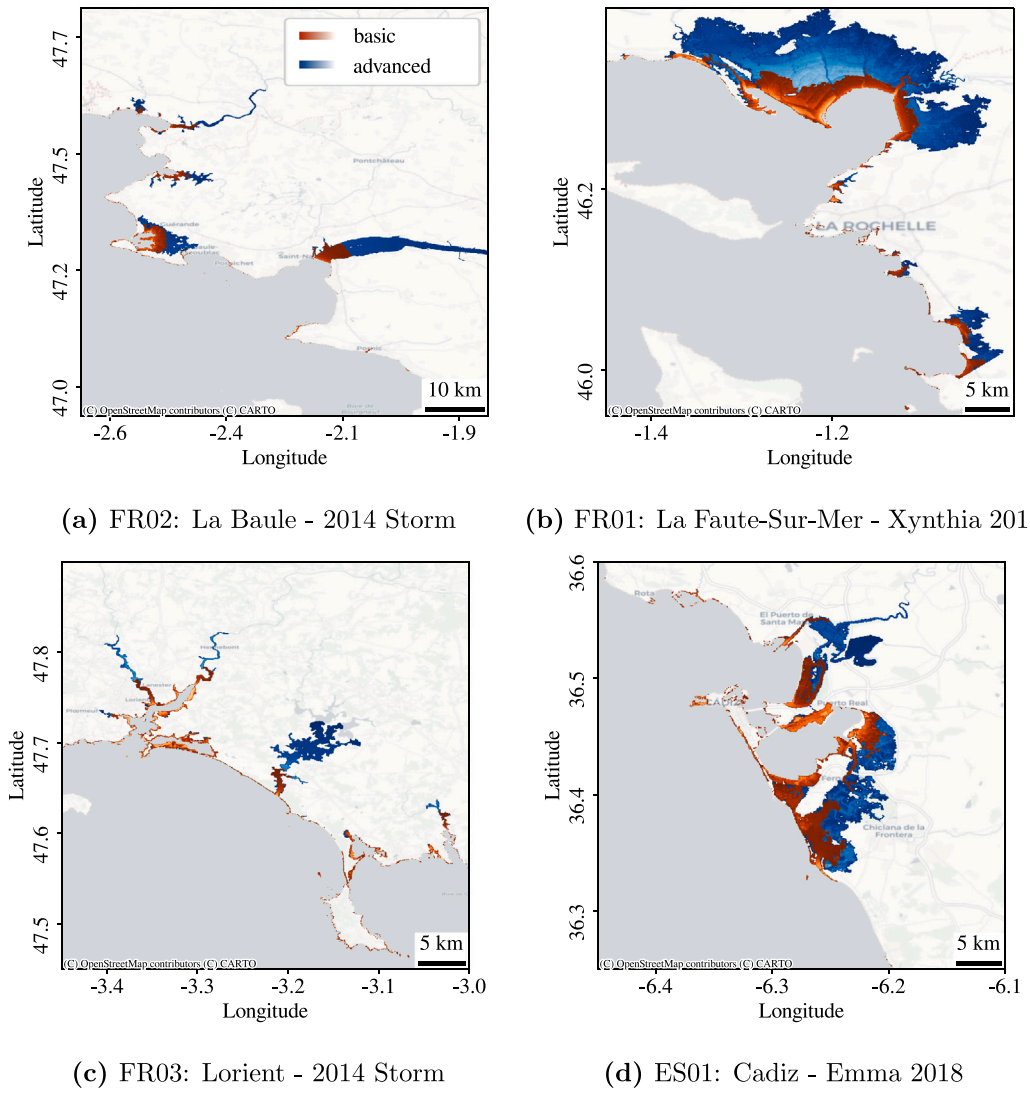

(a) FR02: La Baule - 2014 Storm

(b) FR01: La Faute-Sur-Mer - Xynthia 2010

(c) FR03: Lorient - 2014 Storm

(d) ES01: Cadiz - Emma 2018

Fig. 8. Comparison of the flood extension between the solver options basic (red layer) and advanced (blue layer) for the Atlantic group test cases. The intensity of the colour from dark to light indicates an increase in flood water depth. The flood models correspond to the 50 m resolution, the adapted friction and the basic wave set-up option. The background maps were generated using the OpenStreetMap database available through Python (Open Database License).

In the framework of the present study, the importance of the solver parameter is clearly identified, especially in flood prone areas.

4.3. Resolution and friction influences

The influence of the resolution is important in the North and Baltic Seas and Northern Adriatic group. The reason for the impact of the resolution in this group can be twofold. Firstly, the test cases DE01 and DE02 do not include large flood prone areas nor show a significant contribution of the wave set-up, see Figs. 11 and 10(a). Therefore, the relative resolution influence benefits from the decrease of the impact of the solver and wave set-up. Secondly, there is a loss of representativeness of the local topography at lower resolutions, as highlighted by Seenath (2018) among others. While the resolution of the topography has a limited impact on flat areas, higher topographic features, that protect low elevated areas from flooding, are flattened. In the test cases in Norfolk GB01, Lido delle Nazioni IT03 (IT01 and IT04 are not shown because they are similar to IT03), Wismar DE02 and Warnemunde DE01, areas with flattened topographic features are identifiable, while relatively non-existent in the other test cases (not shown). For each of these test cases, the cross-sections of the topography support this finding, because the most elevated portion of topographic features is smoothed between 25 and 100 m grids, see Fig. 5 for the cross-sections location and Fig. 12 for the topographic profiles. High features in the 25 m resolution grid are able to block the propagation of the water inland, either at the coastline (DE01, DE02, GB01) or further inland (IT03), while their absence at coarser resolutions allows the the water to inundate landward zones. Thus, the change of resolution will likely have a larger effect on areas with small elevation features.

The impact of the resolution on the LISFLOOD-FP model was investigated by Savage et al. (2016) for a fluvial flood. In their work, the grid resolution was compared with the hydrographic accuracy, the river and plain friction as well as with the topography accuracy. From their analysis, the grid resolution was the main influencing factor when considering the local water depth and inundation timing, but not when considering the flood extent for which there is a significant impact of the hydrograph data and bottom friction. Concerning coastal flooding, Brown et al. (2007), Lewis et al. (2011), Smith et al. (2011) also highlighted a lesser influence of the friction than of the forcing

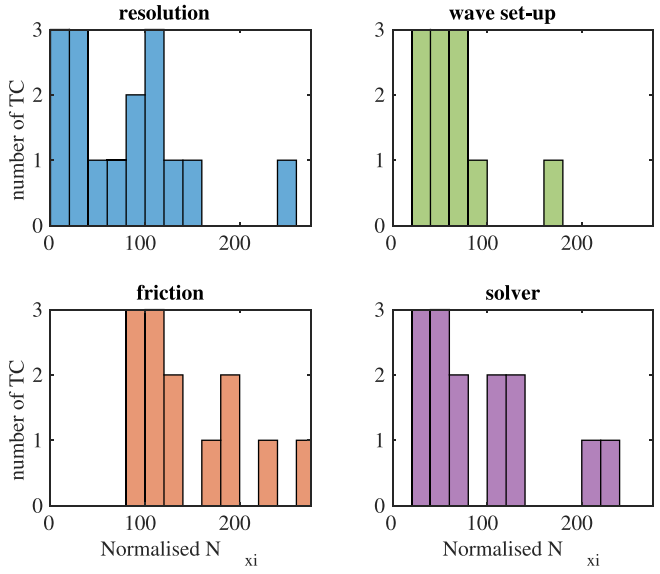

Fig. 9. Histograms of N_{xi} normalised by M_{xi} for each parameter. The x-axis and y-axis correspond to the value of N_{xi} in %, with a bin width of 20%, and the number of associated test cases, respectively.

conditions. In the present study only the test case PL01 at Swijnouscie shows a relative influence of the friction. This difference of relevance of the friction configuration could be linked to the variation in the amplitude imposed in the forcing data during the analyses, possibly higher for coastal than fluvial flooding. In the fluvial case of Savage et al. (2016), the hydrograph variation is contained within 40% of the original data, while in the present cases, an increase of the total water level of more than 200% can be expected between the null and basic options (estimation based on the maximal water depth at the coastline). The exception of the test case PL01 could be due to the particular configuration of the area with the presence of the inner lagoon, favouring the propagation when reached by the water, as in the models with the lower friction options. Overall, the friction does not influence the flood result in comparison with the other considered parameters and for the selected test cases. The isolated result of the test case PL01 illustrates how a local setting can impact a global analysis, and thus bounding the global result to the selected test cases.

4.4. Environmental indicator clustering

An effort to connect the result of the sensitivity analysis to morphological factors specific of each test case was previously made and discussed in Sections 4.1 and 4.2, mainly relating the influence of the wave set-up to Mediterranean hydrodynamic conditions and the impact of the solver to the extension of flood prone area of the specific test-cases. Aiming for more generic conclusions and thus connecting the sensitivity results to environmental characteristics of the site, the test cases were grouped by similar environment indicators by performing a second k-means clustering method on available indicators and proxy potentially impacting the flooded areas. If this second clustering is similar to that of the sensitivity results, some said connections could be speculated. Three morphological indicators were used: the flood prone area extent as proxy of the general elevation of the site, the median coastline elevation and gradient slope extracted from the 25 m grids, and the wave set-up contribution wsu^* as ocean–land interaction indicator. These factors were normalised using the maximal values across the test cases. However, the clusters generated by these parameters of the test cases, Fig. 13, do not directly correlate with the clusters based on the sensitivity analysis. At the exception of the wave set-up, the characteristics of the storm events, thus the boundary condition of the models, were not isolated and included in this exercise. One could expect a combined influence of both the morphological parameter related to the site and the characteristics of the storm. Conversely, storm characteristics are normally consistent on site, so it is not surprising to note that the three test cases for three different events at Lido delle Nazioni (IT01, IT03, IT04) are always grouped together. The discrepancy between the clustering from the sensitivity analysis and the specific indicators of the test cases demonstrates a more complex relationship between these two aspects of the analysis and highlights its limitation. Indeed, following a global analysis, some concessions were made to represent the morphological factors specific to each test case, such as a unique slope and coastline elevation to represent a 100 km-long test case, and thus the result is bounded to the limitation of the data used.

4.5. Influence on the computational time

In addition to the sensitivity to the parameters discussed above, another important factor is the computational time (CT). This is especially important when developing global models. CT depends on the computation set-up, the flood model configuration, and the specific flood event: a larger and longer event will need more time than a shorter one, etc. In the present study, the computational time significantly varied depending on the configuration of the flood model. The resolution was the most significant, with, on average, the CT multiplying by 4 when changing from 100 m to 50 m; and by 32 from 100 m to 25 m. More specifically, the impact of the resolution on the CT also depended on the option of the solver, as, with the 25 m configuration and for a few test cases, the acceleration solver could multiply the CT by more than 80 times. Subsequently, on average, the acceleration solver doubled CT in comparison with the flow limited solver. However, the influence of the solver on the CT also depended on the resolution. By comparing the two solver options, the CT was slightly increased at 100 m, was multiplied by 1.5 for 50 m, and on average was more than tripled at 25 m with the acceleration solver. On the contrary, the boundary condition and friction options on average did not have much impact on the CT. These differences highlight the importance of the efficiency-quality balance and the benefit of knowing how each parameter influences the result.

4.6. Limitations

The analysis presented in this work shows some limitations. Firstly, the quality of the flood model results is constrained by the availability and quality of input data such as boundary conditions, nearshore bathymetry, and DEM. The main source of uncertainty lies in the resolution and vertical accuracy (< 4 m) of the DEM, which influences the flood computation. The second source of uncertainty, but no less importantly, is the approach adopted to compute the TWL time series used to force the flood model. In this regard, the linear addition of TWL components (i.e., mean sea level variability, storm surges, wave contributions, or tides in Mediterranean cases) potentially neglects the nonlinear interaction between different components. Additionally, the SSH component is generally underestimated in the dataset used in this work, especially during peak events (e.g., -23 cm in the Emma storm or −0.45cm for the Delft storm reported by Irazoqui Apecechea et al., 2023), in contrast with very high-resolution storm-specific models (e.g., Bertin et al., 2014 for Xynthia or Amores et al. (2020) for Gloria). Furthermore, the estimation of wave contribution is also subject to limitations. Firstly, this work takes into account only the wave setup contribution, excluding swash excursion for a complete calculation of wave run-up (wave setup + swash), which leads to an underestimation of the final wave contribution to TWL on the coast. Secondly, processes associated to the wave propagation in the nearshore area (diffraction, refraction, dissipation by bottom

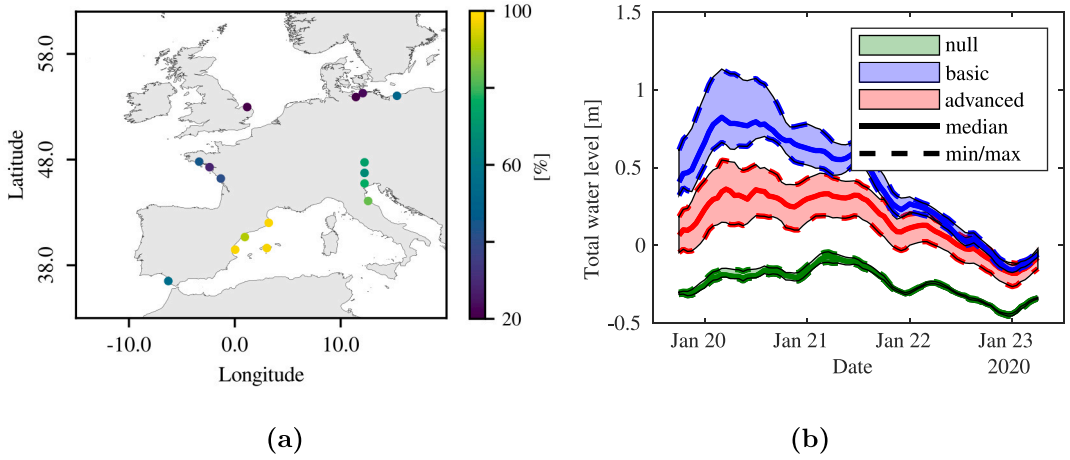

Fig. 10. 10(a): Median of the relative wave set-up contribution (%) for each test case from the maximum water depth at the coastline. 10(b) Total water level time series for the test case ES02: Castellon (ES) - Gloria 2020.

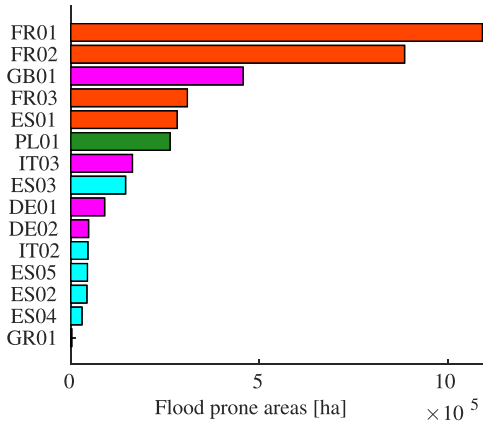

Fig. 11. Estimation of the flood prone areas using the wetland, beach, dune and river bank classes defined by the LU/LC coastal Zone 2018 for each test cases (as IT01, IT03 and IT04 are at the same site only IT03 is displayed). The colour of each bar matches the corresponding cluster identified in Fig. 4.

friction and wave breaking) play an important role in the final wave setup computation, and the modelling approach used does not solve these processes in complex nearshore areas (e.g., presence of enclosed embayments, delta mouth bars, or rocky islands). Moreover, the semi-empirical formulation used to compute wave setup is a simplistic approach. In this study, the closest coastal point, mostly located in shallow water depth, was used to obtain the wave bulk parameter to feed Stockdon's formulation for wave setup, while the formula was originally derived for offshore or deep water wave parameters. This could also result in a systematic misrepresentation of the wave setup contribution. Including the beach slope as a primary variable in wave setup improves the representation of wave setup compared to the formulation proposed by Holman and Sallenger (1985), which only accounts for significant wave height. However, it requires a high accuracy and resolution topo-bathymetric dataset generally scarce or not available for large-scale or regional analysis. In this sense, although the method used to calculate the beach slope in this study is a good approximation to represent spatial variability of the slope in the test cases (see Fig. A.17), the use of the gradient slope instead of cross-shore slope could imply a systematic overestimation of slopes and consequently an amplification of wave setup contribution. Therefore, it is acknowledged that the values obtained may differ from the real ones. In this regard, an assessment of the slope computation method was conducted by comparing the average of the cross-shore slope derived from cross-shore profiles extracted from the DEM and the gradient slope using ten profiles per site of the main sites (Norfolk, Lido delle Nazioni, Ebro, Cadiz, La Faute Sur Mer and Wismar). The analysis shows an average ratio (Cross-shore slope / Gradient slope) of 0.66 with a standard deviation of 0.36, indicating a general overestimation of the slope used in this work. The gradient slope and cross-shore slope show a high correlation (0.73, p-Value =8e-11) indicating that the gradient methods reflect the spatial variability of the real cross-shore slope. In addition, the correlation between Cross-shore slope / Gradient slope ratio and the gradient slope show a low correlation (−0.1, p-Value = 0.36). These results reveal a systematic error, the overestimation of the slope and therefore wave set up contribution, without invalidating the sensitivity analysis performed in this study. Beyond this aspect there are other limitations, for instance the flood model does not integrate the river dynamics or discharge which could modify the flood propagation in estuaries and deltaic mouths (Kumbier et al., 2018; Bevacqua et al., 2020). In addition, coastal protection structures, not-caught by the DEM, were not integrated into the models while they could lead to significant differences and uncertainties on the resulting flood maps (Vousdoukas et al., 2016, 2018; Paprotny et al., 2019). This could become an interesting additional key parameter to integrate in a future extension of the work as the analysis considers only a four not-exhaustive list of parameters. Second, as stated in the introduction, the results of the sensitivity analysis are controlled by the method and sample used. In the present study, even if the analysis covered 17 test-cases, four parameters are considered with a sampling size varying between two and four options. While some parameters are limited in their sampling, the range of the numerical parameters could benefit from an extension such as the DEM resolution as performed by Savage et al. (2016). Indeed, an increasing in sampling size could improve the study.

5. Conclusions

With the aim of a European-scale sensitivity analysis of flood models through an assessment of the relative influence of parameters such as the grid resolution, the numerical floodplain solver, the friction coefficient and the wave set-up estimation, seventeen test cases were reproduced with multiple configurations of the LISFLOOD-FP model.

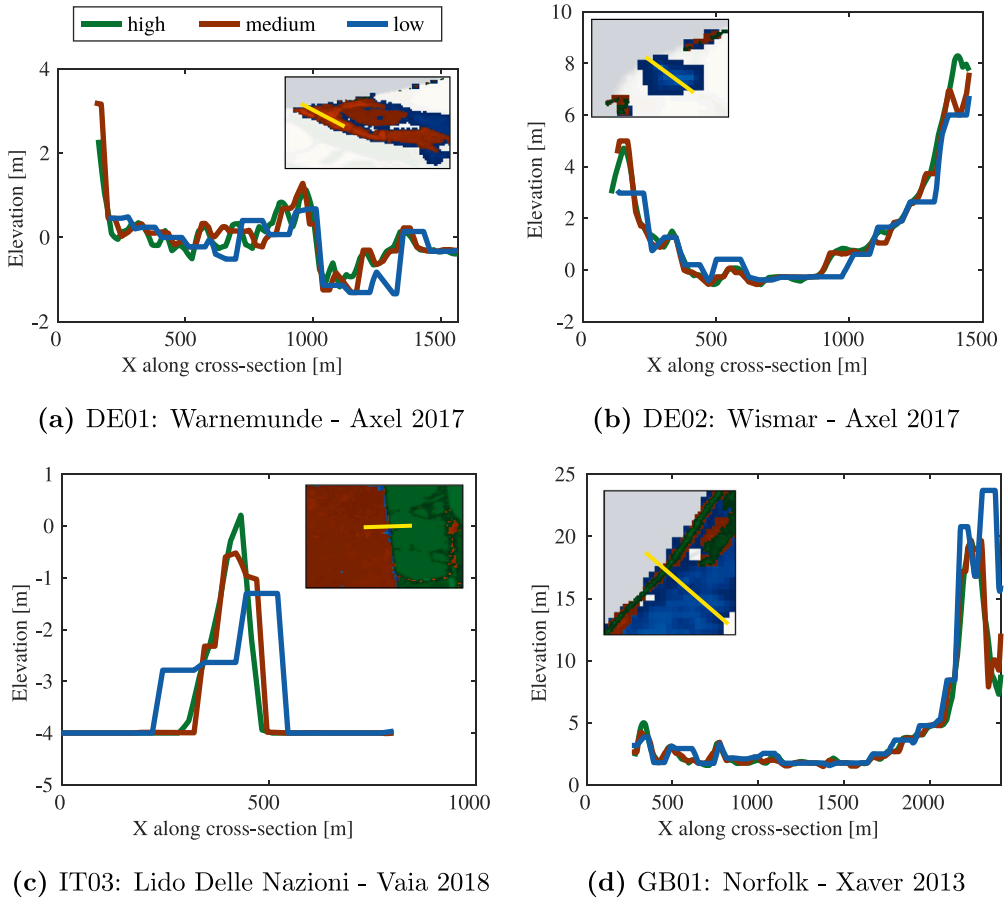

Fig. 12. Elevation profiles along cross-sections for topographic grids with 25, 50 and 100 m resolution (respectively green, red and blue lines). The intensity of the colour from dark to light indicates an increase in flood water depth. The inset maps correspond to the yellow boxes of Fig. 5 and the yellow lines to the cross-sections.

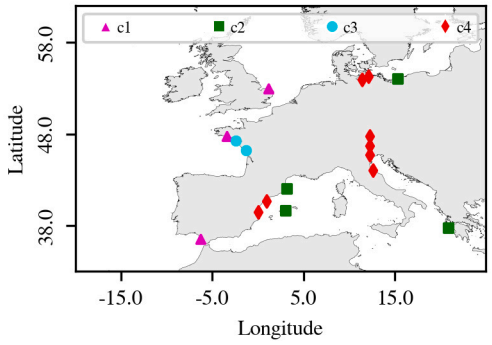

Fig. 13. Clusters identified by the k-means clustering method with the environmental factors as input.

One-Driver-At-a-Time and variance based sensitivity methods were applied to both the maximum flood area and maximum water volume giving similar, thus robust, results. The test cases were sorted through a k-means clustering method performed on the sensitivity results, identifying clusters with similar sensitivity to their configuration. The floodplain solver was highlighted as influencing most of the test cases, and especially for the simulations on the Atlantic coasts which include large flood prone areas. As consequences of the Mediterranean oceanographic conditions, the Mediterranean test cases (except those at Lido Delle Nazioni, IT) were strongly sensitive to the wave set-up estimation, emphasising its relative importance in this region without discarding its relevance in the Atlantic and North Shelf regions. The influence of the grid resolution increased for the test cases in the North and Baltic Seas and one site in North Adriatic (Lido delle Nazioni). While being less exposed to the previously mentioned conditions, these test cases were affected by the obliteration of small protecting topographic features caused by the low resolution. This led to additional flooded areas in 100 m resolution models which remained dried at 25 m, and thus highlighting the limitation of using coarse grids. Globally the friction option weakly influenced the output of the flood models, as previously highlighted by other works. Only one test case proved to be relatively sensitive to this parameter, also highlighting how the local environment can affect global analyses. It is also important to stress a co-dependence of the parameters, particularly in the case of the friction parameter. Finally, targeting a more generic conclusion to attribute the parameter's influences to environmental indicator, a k-means clustering algorithm was applied to morphological and wave set-up factors specific to each test cases. The difference between the clustering from the test case factors and the sensitivity results revealed a more complex relationship between the test case and its model configuration, that also could be due to the limitation arising from the scale of the analysis.

Collecting information on the influence of each parameter gave an ensemble view of the importance of the regional environment; an outlook that could be used to develop local and global models as

it indicates which parameters to prioritise during the configuration process. From this perspective, any attempt to build a flood model for European scale, should give special care in using the solver option and the boundary condition. It should also be noted that both the resolution and the floodplain solver have a computational cost to be considered during model development as they greatly multiplied the computational time when the most advance options are used. Thus, it will be recommended to adapt the flood model configuration along the European shore depending of the need of each areas. It should be highlighted that the present analysis is limited by the singularity of the test cases, meaning that, with the exception of three test cases, all the other test cases concern only one event, restraining sensitivity analysis to a unique storm condition. In addition, the analyses were performed on four parameters with limited sample. As future works, increasing the number of parameters and their sampling size could only be beneficial, such as the integration of coastal protection structures or adding more resolution options. It will be also interesting to investigate the difference between the method applied for the analysis.

CRediT authorship contribution statement

Marine Le Gal: Writing – review & editing, Writing – original draft, Validation, Software, Methodology, Investigation, Formal analysis, Conceptualization. **Tomás Fernández-Montblanc:** Writing – review & editing, Writing – original draft, Validation, Supervision, Software, Methodology, Investigation, Formal analysis, Conceptualization. **Juan Montes Perez:** Writing – review & editing, Resources. **Enrico Duo:** Writing – review & editing, Resources. **Paola Souto Ceccon:** Resources. **Paolo Ciavola:** Writing – review & editing, Supervision, Funding acquisition. **Clara Armaroli:** Funding acquisition, Project administration, Writing – review & editing.

Declaration of competing interest

The authors declare that they have no known competing financial interests or personal relationships that could have appeared to influence the work reported in this paper.

Data availability

Data will be made available on request.

Acknowledgements

This work was performed within the framework of the ECFAS (A Proof-of-Concept for the Implementation of a European Copernicus Coastal Flood Awareness System) project. ECFAS has received funding from the EU H2020 research and innovation program under Grant Agreement No 101004211. Marine Le Gal also benefited from the "Go for IT" grant (Area 04 – Scienze della Terra) from the Fondazione CRUI under the responsibility of P. Ciavola. J. Montes has a postdoctoral contract Margarita Salas at the University of Cadiz from the Ministry of Universities of Spain, funded by the European Union-NextGenerationEU.

Appendix. Sensitivity analysis results for each test case

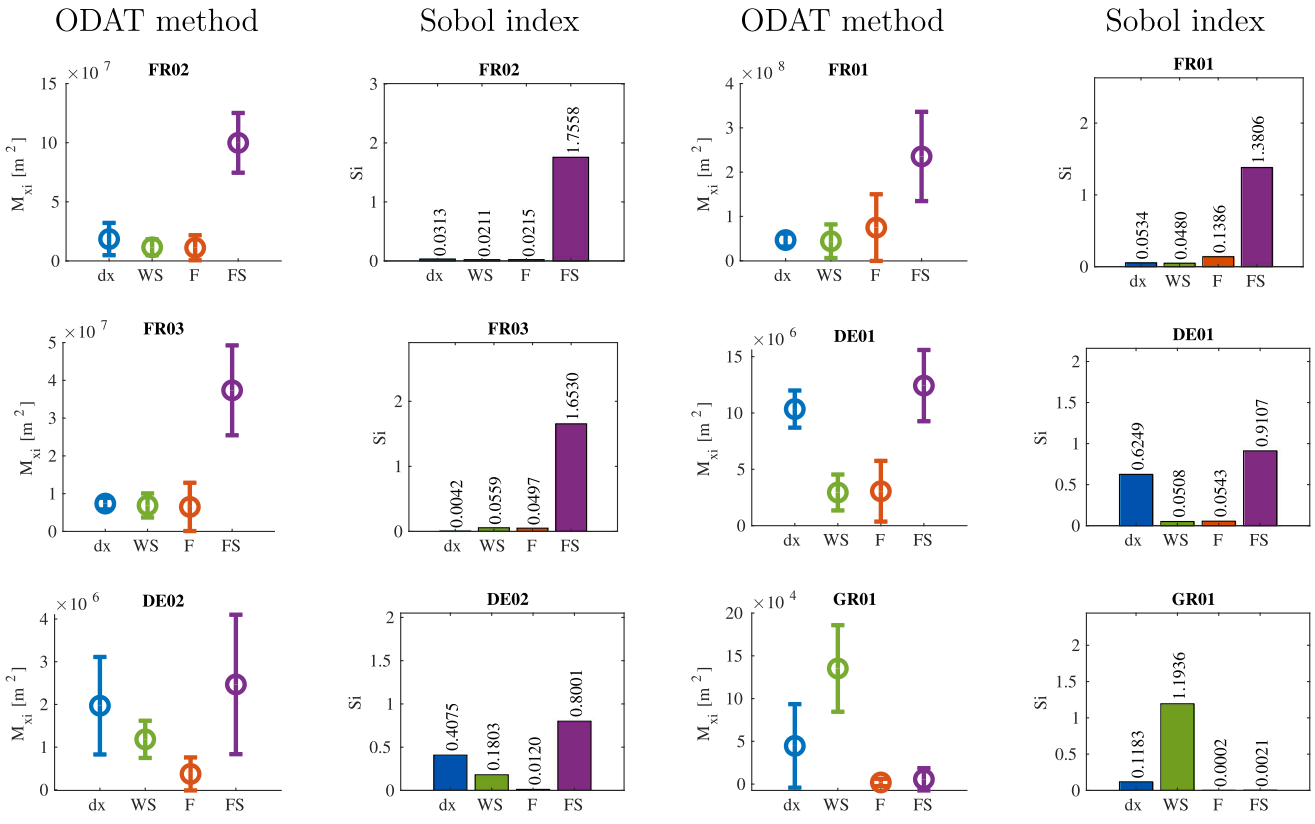

Fig. A.14. ODAT (M_{xi} and N_{xi}) and Sobol first index results from the Maximal Flood Area, for each test case, see Table 1 for the corresponding test case ID.

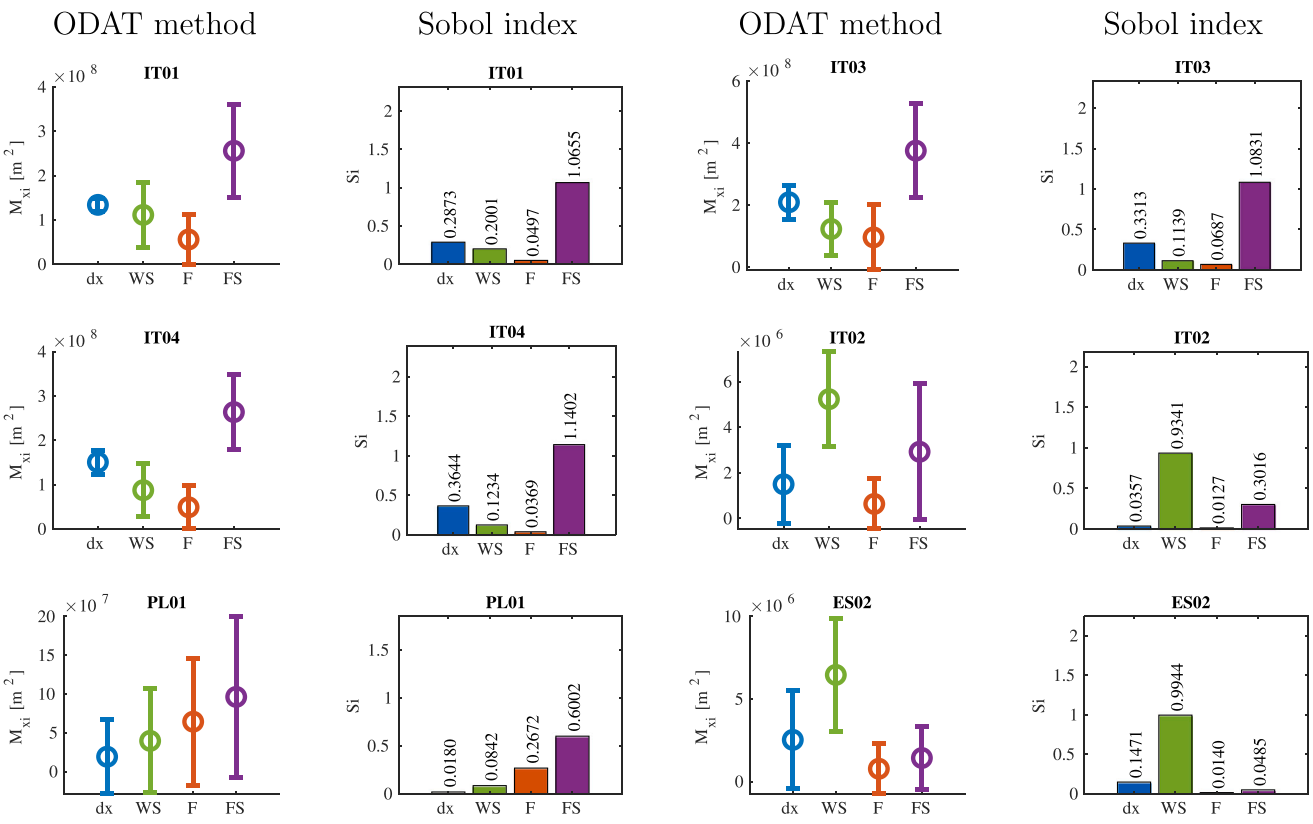

Fig. A.15. Same as Fig. A.14.

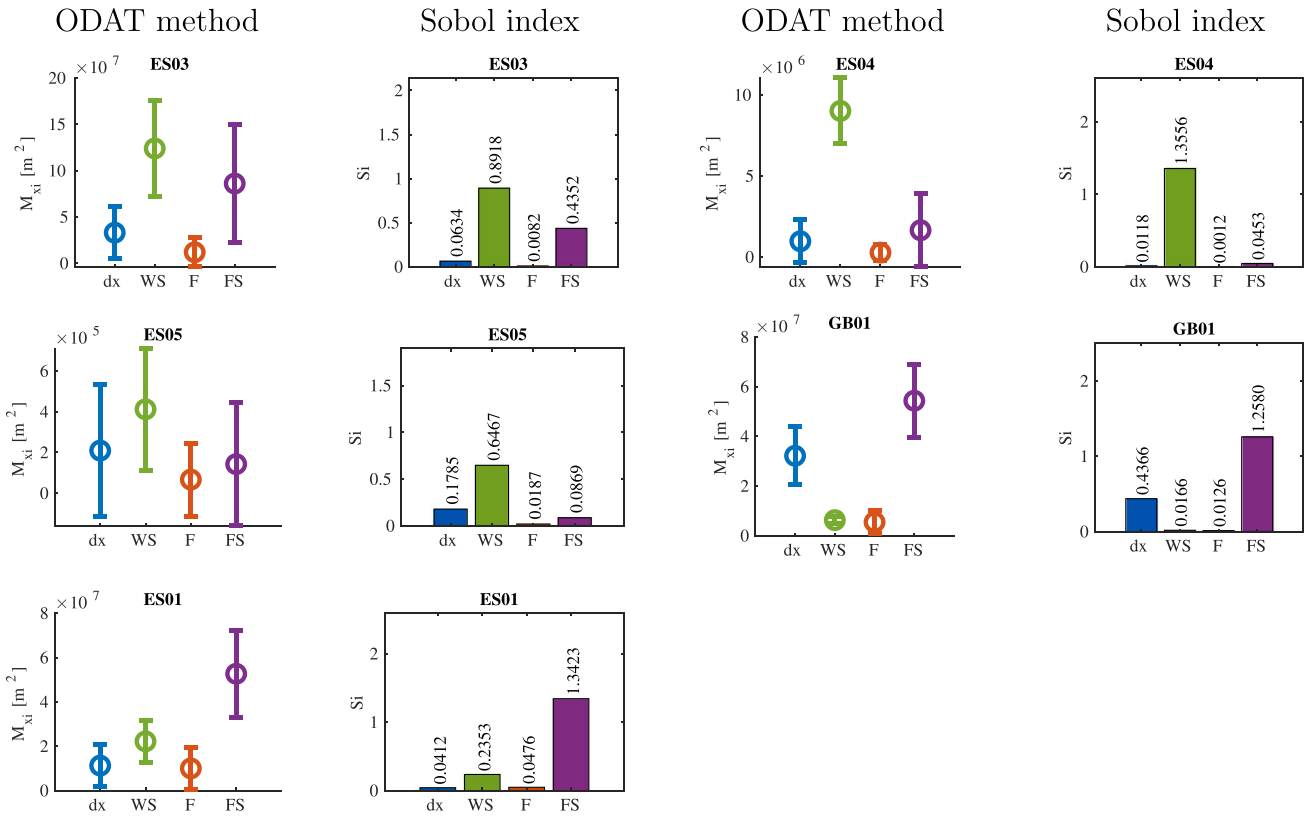

Fig. A.16. Same as Fig. A.14.

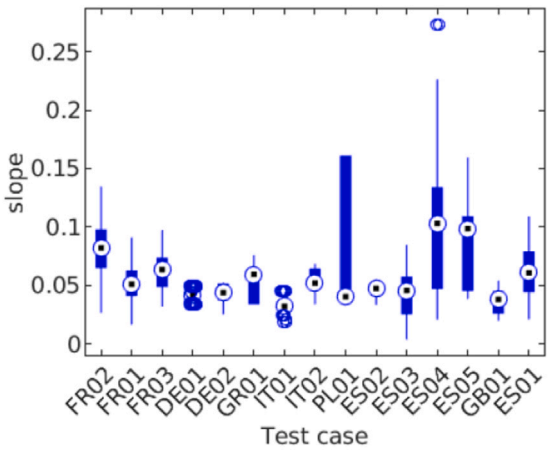

Fig. A.17. Box plot summarising the statistics associated to the applied foreshore slope at each site.

References

Alipour, A., Jafarzadegan, K., Moradkhani, H., 2022. Global sensitivity analysis in hydrodynamic modeling and flood inundation mapping. Environ. Model. Softw. 152, 105398. http://dx.doi.org/10.1016/j.envsoft.2022.105398.

Amores, A., Marcos, M., Carrió, D.S., Gómez-Pujol, L., 2020. Coastal impacts of Storm Gloria (January 2020) over the north-western Mediterranean. Nat. Hazards Earth Syst. Sci. 20 (7), 1955–1968. http://dx.doi.org/10.5194/nhess-20-1955-2020.

Andersen, O.B., Knudsen, P., 2009. DNSC08 mean sea surface and mean dynamic topography models. J. Geophys. Res. 114 (C11), C11001. http://dx.doi.org/10.1029/2008JC005179.

Athanasiou, P., van Dongeren, A., Giardino, A., Vousdoukas, M., Gaytan-Aguilar, S., Ranasinghe, R., 2019. Global distribution of nearshore slopes with implications for coastal retreat. Earth Syst. Sci. Data 11 (4), 1515–1529. http://dx.doi.org/10.5194/essd-11-1515-2019.

Barnard, P.L., van Ormondt, M., Erikson, L.H., Eshleman, J., Hapke, C., Ruggiero, P., Adams, P.N., Foxgrover, A.C., 2014. Development of the coastal storm modeling system (CoSMoS) for predicting the impact of storms on high-energy, active-margin coasts. Nat. Hazards 74 (2), 1095–1125. http://dx.doi.org/10.1007/s11069-014-1236-y.

Bates, P.D., Dawson, R.J., Hall, J.W., Horritt, M.S., Nicholls, R.J., Wicks, J., Hassan, M., 2005. Simplified two-dimensional numerical modelling of coastal flooding and example applications. Coast. Eng. 52 (9), 793–810. http://dx.doi.org/10.1016/j.coastaleng.2005.06.001.

Bates, P., De Roo, A., 2000. A simple raster-based model for flood inundation simulation. J. Hydrol. 236 (1–2), 54–77. http://dx.doi.org/10.1016/S0022-1694(00)00278-X.

Bates, P.D., Horritt, M.S., Fewtrell, T.J., 2010. A simple inertial formulation of the shallow water equations for efficient two-dimensional flood inundation modelling. J. Hydrol. 387 (1–2), 33–45. http://dx.doi.org/10.1016/j.jhydrol.2010.03.027.

Bates, P.D., Trigg, M., Neal, J., Dabrowa, A., 2013. LISFLOOD User Manual-FP. School of Geographical Sciences, University of Bristol, Bristol, UK, https://www.bristol.ac.uk/media-library/sites/geography/migrated/documents/lisflood-manual-v5.9.6.pdf.

Bertin, X., Li, K., Roland, A., Zhang, Y.J., Breilh, J.F., Chaumillon, E., 2014. A modeling-based analysis of the flooding associated with Xynthia, central Bay of Biscay. Coast. Eng. 94, 80–89. http://dx.doi.org/10.1016/j.coastaleng.2014.08.013.

Bevacqua, E., Vousdoukas, M.I., Shepherd, T.G., Vrac, M., 2020. Brief communication: The role of using precipitation or river discharge data when assessing Global Coastal compound flooding. Nat. Hazards Earth Syst. Sci. 20 (6), 1765–1782. http://dx.doi.org/10.5194/nhess-20-1765-2020.

Brown, J.D., Spencer, T., Moeller, I., 2007. Modeling storm surge flooding of an urban area with particular reference to modeling uncertainties: A case study of Canvey Island, United Kingdom. Water Resour. Res. 43 (6), http://dx.doi.org/10.1029/2005WR004597.

Calafat, F.M., Wahl, T., Tadesse, M.G., Sparrow, S.N., 2022. Trends in Europe storm surge extremes match the rate of sea-level rise. Nature 603 (7903), 841–845. http://dx.doi.org/10.1038/s41586-022-04426-5.

Chow, V.T., 1959. Open-Channel Hydraulics. McGraw-Hill, New York, p. 728.

Clementi, E., Aydogdu, A., Goglio, A.C., Pistoia, J., Escudier, R., Drudi, M., Grandi, A., Mariani, A., Lyubartsev, V., Lecci, R., Cretí, S., Coppini, G., Masina, S., Pinardi, N., 2021. Mediterranean sea physical analysis and forecast (CMEMS MED-currents, EAS6 system): MEDSEA_ANALYSISFORECAST_PHY_006_013. http://dx.doi.org/10.25423/CMCC/MEDSEA_ANALYSISFORECAST_PHY_006_013_EAS6.

Copernicus Marine Service, 2017. Atlantic-Iberian Biscay Irish- ocean physics analysis and forecast. http://dx.doi.org/10.48670/MOI-00027.

Copernicus Marine Service, 2018. Baltic sea physics reanalysis. http://dx.doi.org/10.48670/MOI-00013.

Copernicus Marine Service, 2020a. Atlantic -Iberian Biscay Irish- ocean wave reanalysis. http://dx.doi.org/10.48670/MOI-00030.

Copernicus Marine Service, 2020b. Atlantic-Iberian Biscay Irish- ocean physics reanalysis. http://dx.doi.org/10.48670/MOI-00029.

Copernicus Marine Service, 2020c. Baltic sea wave hindcast. http://dx.doi.org/10.48670/MOI-00014.

Criado-Aldeanueva, F., Del Río Vera, J., García-Lafuente, J., 2008. Steric and mass-induced Mediterranean sea level trends from 14 years of altimetry data. Glob. Planet. Change 60 (3–4), 563–575. http://dx.doi.org/10.1016/j.gloplacha.2007.07.003.

de Moel, H., Asselman, N.E.M., Aerts, J.C.J.H., 2012. Uncertainty and sensitivity analysis of coastal flood damage estimates in the west of the Netherlands. Nat. Hazards Earth Syst. Sci. 12 (4), 1045–1058. http://dx.doi.org/10.5194/nhess-12-1045-2012.

Dodet, G., Melet, A., Ardhuin, F., Bertin, X., Idier, D., Almar, R., 2019. The contribution of wind-generated waves to coastal sea-level changes. Surv. Geophys. 40 (6), 1563–1601. http://dx.doi.org/10.1007/s10712-019-09557-5.

Escudier, R., Clementi, E., Omar, M., Cipollone, A., Pistoia, J., Aydogdu, A., Drudi, M., Grandi, A., Lyubartsev, V., Lecci, R., Cretí, S., Masina, S., Coppini, G., Pinardi, N., 2020. Mediterranean sea physical reanalysis (CMEMS MED-Currents, E3R1 system): MEDSEA_MULTIYEAR_PHY_006_004. http://dx.doi.org/10.25423/CMCC/MEDSEA_MULTIYEAR_PHY_006_004_E3R1.

European Space Agency and Airbus, 2022. Copernicus DEM. http://dx.doi.org/10.5270/ESA-c5d3d65.

Fernández-Montblanc, T., Duo, E., Ciavola, P., 2020. Dune reconstruction and revegetation as a potential measure to Decrease Coastal erosion and flooding under extreme storm conditions. Ocean Coast. Manag. 188, 105075. http://dx.doi.org/10.1016/j.ocecoaman.2019.105075.

Fernández-Montblanc, T., Gómez-Enri, J., Ciavola, P., 2020. The role of mean sea level annual cycle on extreme water levels along European coastline. Remote Sens. 12 (20), http://dx.doi.org/10.3390/rs12203419.

Fernández-Montblanc, T., Vousdoukas, M., Ciavola, P., Voukouvalas, E., Mentaschi, L., Breyiannis, G., Feyen, L., Salamon, P., 2019. Towards robust Pan-European storm surge forecasting. Ocean Model. 133, 129–144. http://dx.doi.org/10.1016/j.ocemod.2018.12.001.

Forzieri, G., Feyen, L., Russo, S., Vousdoukas, M., Alfieri, L., Outten, S., Migliavacca, M., Bianchi, A., Rojas, R., Cid, A., 2016. Multi-hazard assessment in Europe under climate change. Clim. Change 137 (1–2), 105–119. http://dx.doi.org/10.1007/s10584-016-1661-x.

Gallien, T., Kalligeris, N., Delisle, M.-P., Tang, B.-X., Lucey, J., Winters, M., 2018. Coastal flood modeling challenges in defended urban backshores. Geosciences 8 (12), 450. http://dx.doi.org/10.3390/geosciences8120450.

García-García, D., Chao, B.F., Boy, J.P., 2010. Steric and mass-induced sea level variations in the Mediterranean Sea revisited. J. Geophys. Res.: Oceans 115 (C12), 2009JC005928. http://dx.doi.org/10.1029/2009JC005928.

Genovese, E., Przyluski, V., 2013. Storm surge disaster risk management: The Xynthia case study in France. J. Risk Res. 16 (7), 825–841. http://dx.doi.org/10.1080/13669877.2012.737826.

Grilli, A.R., Westcott, G., Grilli, S.T., Spaulding, M.L., Shi, F., Kirby, J.T., 2020. Assessing Coastal hazard from extreme storms with a phase resolving wave model: Case study of Narragansett, RI, USA. Coast. Eng. 160, 103735. http://dx.doi.org/10.1016/j.coastaleng.2020.103735.

Hall, J.W., Tarantola, S., Bates, P.D., Horritt, M.S., 2005. Distributed sensitivity analysis of flood inundation model calibration. J. Hydraul. Eng. 131 (2), 117–126. http://dx.doi.org/10.1061/(ASCE)0733-9429(2005)131:2(117).

Hinkel, J., Lincke, D., Vafeidis, A.T., Perrette, M., Nicholls, R.J., Tol, R.S.J., Marzeion, B., Fettweis, X., Ionescu, C., Levermann, A., 2014. Coastal flood damage and adaptation costs under 21st century sea-level rise. Proc. Natl. Acad. Sci. USA 111 (9), 3292–3297. http://dx.doi.org/10.1073/pnas.1222469111.

Holman, R.A., Sallenger, A.H., 1985. Setup and swash on a natural beach. J. Geophys. Res. 90 (C1), 945. http://dx.doi.org/10.1029/JC090iC01p00945.

Idier, D., Bertin, X., Thompson, P., Pickering, M.D., 2019. Interactions between mean sea level, tide, surge, waves and flooding: Mechanisms and contributions to sea level variations at the coast. Surv Geophys 40 (6), 1603–1630. http://dx.doi.org/10.1007/s10712-019-09549-5.

Innerbichler, F., Kreisel, A., Gruber, C., 2021. Coastal Zones Nomenclature Guideline. Technical Report, Copernicus Land Monitoring Service.

Irazoqui Apecechea, M., Melet, A., Armaroli, C., 2023. Towards a pan-European coastal flood awareness system: Skill of extreme sea-level forecasts from the Copernicus Marine Service. Front. Mar. Sci. 9, 1091844. http://dx.doi.org/10.3389/fmars.2022.1091844.

Kalakan, C., Sriariyawat, A., Naksuksakul, S., Rasmeemasmuang, T., 2016. Sensitivity analysis of coastal flooding to geographical factors: Numerical model study on idealized beaches. EJ 20 (1), 1–15. http://dx.doi.org/10.4186/ej.2016.20.1.1.

Kiesel, J., Lorenz, M., König, M., Gräwe, U., Vafeidis, A.T., 2023. Regional assessment of extreme sea levels and Associated Coastal flooding along the German Baltic Sea coast. Nat. Hazards Earth Syst. Sci. 23 (9), 2961–2985. http://dx.doi.org/10.5194/nhess-23-2961-2023.

Kıyıcı, E., 2019. Sensitivity analysis of 2-D flood inundation model LISFLOOD-FP with respect to spatial resolution and roughness parameter unpublished msc thesis in civil engineering, middle east technical university, https://etd.lib.metu.edu.tr/upload/12623195/index.pdf.

Kolen, B., Slomp, R., Jonkman, S., 2013. The impacts of storm Xynthia February 27-28, 2010 in France: Lessons for flood risk management: Impacts of storm Xynthia. J. Flood Risk Manage 6 (3), 261–278. http://dx.doi.org/10.1111/jfr3.12011.

Korres, G., Ravdas, M., Zacharioudaki, A., Denaxa, D., Sotiropoulou, M., 2021a. Mediterranean sea waves analysis and forecast (CMEMS med-waves, MedWAM3 system): MEDSEA analysisforecast WAV 006 017. http://dx.doi.org/10.25423/CMCC/MEDSEA_ANALYSISFORECAST_WAV_006_017_MEDWAM3.

Korres, G., Ravdas, M., Zacharioudaki, A., Denaxa, D., Sotiropoulou, M., 2021b. Mediterranean sea waves reanalysis (CMEMS med-waves, MedWAM3 system): MEDSEA_MULTIYEAR_WAV_006_012. http://dx.doi.org/10.25423/CMCC/MEDSEA_MULTIYEAR_WAV_006_012.

Kumbier, K., Carvalho, R.C., Vafeidis, A.T., Woodroffe, C.D., 2018. Investigating compound flooding in an estuary using hydrodynamic modelling: A case study from the Shoalhaven River, Australia. Nat. Hazards Earth Syst. Sci. 18 (2), 463–477. http://dx.doi.org/10.5194/nhess-18-463-2018.

Le Gal, M., Fernández-Montblanc, T., Duo, E., Montes Perez, J., Cabrita, P., Souto Ceccon, P., Gastal, V., Ciavola, P., Armaroli, C., 2023. A new European coastal flood database for low–medium intensity events. Nat. Hazards Earth Syst. Sci. 23 (11), 3585–3602. http://dx.doi.org/10.5194/nhess-23-3585-2023.

Leon, J.X., Heuvelink, G.B.M., Phinn, S.R., 2014. Incorporating DEM uncertainty in coastal inundation mapping. PLoS One 9 (9), e108727. http://dx.doi.org/10.1371/journal.pone.0108727.

Lewis, M., Bates, P., Horsburgh, K., Neal, J., Schumann, G., 2013. A storm surge inundation model of the northern Bay of Bengal using publicly available data: A Bay of Bengal storm surge inundation model. Q.J.R. Meteorol. Soc. 139 (671), 358–369. http://dx.doi.org/10.1002/qj.2040.

Lewis, M., Horsburgh, K., Bates, P., Smith, R., 2011. Quantifying the uncertainty in future coastal flood risk estimates for the U.K. J. Coast. Res. 276, 870–881. http://dx.doi.org/10.2112/JCOASTRES-D-10-00147.1.

Lloyd, S., 1982. Least squares quantization in PCM. IEEE Trans. Inform. Theory 28 (2), 129–137. http://dx.doi.org/10.1109/TIT.1982.1056489.

Luján López, A., 2022. Las siniestralidades de Gloria. Consor Seguros revista digital.

Lyard, F.H., Allain, D.J., Cancet, M., Carrère, L., Picot, N., 2021. FES2014 global ocean tide atlas: Design and performance. Ocean Sci. 17 (3), 615–649. http://dx.doi.org/10.5194/os-17-615-2021.

Lyddon, C.E., Brown, J.M., Leonardi, N., Plater, A.J., 2020. Sensitivity of flood hazard and damage to modelling approaches. JMSE 8 (9), 724. http://dx.doi.org/10.3390/jmse8090724.

Marcos, M., Rohmer, J., Vousdoukas, M.I., Mentaschi, L., Le Cozannet, G., Amores, A., 2019. Increased extreme coastal water levels due to the combined action of storm surges and wind waves. Geophys. Res. Lett. 46 (8), 4356–4364. http://dx.doi.org/10.1029/2019GL082599.

Melet, A., Meyssignac, B., Almar, R., Le Cozannet, G., 2018. Under-estimated wave contribution to coastal sea-level rise. Nat. Clim. Change 8 (3), 234–239. http://dx.doi.org/10.1038/s41558-018-0088-y.

Merkens, J.-L., Reimann, L., Hinkel, J., Vafeidis, A.T., 2016. Gridded population projections for the coastal zone under the shared socioeconomic pathways. Glob. Planet. Change 145, 57–66. http://dx.doi.org/10.1016/j.gloplacha.2016.08.009.

Mokrech, M., Kebede, A.S., Nicholls, R.J., Wimmer, F., Feyen, L., 2015. An integrated approach for assessing flood impacts due to future climate and socio-economic conditions and the scope of adaptation in Europe. Clim. Change 128 (3–4), 245–260. http://dx.doi.org/10.1007/s10584-014-1298-6.

Muis, S., Verlaan, M., Winsemius, H.C., Aerts, J.C.J.H., Ward, P.J., 2016. A global reanalysis of storm surges and extreme sea levels. Nature Commun. 7 (1), 11969. http://dx.doi.org/10.1038/ncomms11969.

Neal, J., Villanueva, I., Wright, N., Willis, T., Fewtrell, T., Bates, P., 2012. How much physical complexity is needed to model flood inundation? Hydrol. Process. 26 (15), 2264–2282. http://dx.doi.org/10.1002/hyp.8339.

Olbert, A.I., Comer, J., Nash, S., Hartnett, M., 2017. High-resolution multi-scale modelling of coastal flooding due to tides, storm surges and rivers inflows. A Cork City example. Coast. Eng. 121, 278–296. http://dx.doi.org/10.1016/j.coastaleng.2016.12.006.

Papaioannou, G., Efstratiadis, A., Vasiliades, L., Loukas, A., Papalexiou, S.M., Koukouvinos, A., Tsoukalas, I., Kossieris, P., 2018. An operational method for flood directive implementation in Ungauged Urban Areas. Hydrology 5 (2), 24. http://dx.doi.org/10.3390/hydrology5020024.

Paprotny, D., Morales-Nápoles, O., Jonkman, S.N., 2018. HANZE: A pan-European database of exposure to natural hazards and damaging historical floods since 1870. Earth Syst. Sci. Data 10 (1), 565–581. http://dx.doi.org/10.5194/essd-10-565-2018.

Paprotny, D., Morales-Nápoles, O., Vousdoukas, M.I., Jonkman, S.N., Nikulin, G., 2019. Accuracy of pan-European coastal flood mapping. J. Flood Risk Manag. 12 (2), e12459. http://dx.doi.org/10.1111/jfr3.12459.

Pérez-Gómez, B., García-León, M., García-Valdecasas, J., Clementi, E., Mösso Aranda, C., Pérez-Rubio, S., Masina, S., Coppini, G., Molina-Sánchez, R., Muñoz-Cubillo, A., García Fletcher, A., Sánchez González, J.F., Sánchez-Arcilla, A., Álvarez Fanjul, E., 2021. Understanding sea level processes during Western Mediterranean Storm Gloria. Front. Mar. Sci. 8, 647437. http://dx.doi.org/10.3389/fmars.2021.647437.

Portner, H., Roberts, D., Tignor, M., Poloczanska, E., Mintenbeck, K., Alegria, A., Craig, M., Langsdorf, S., Loschke, S., Moller, V., Okem, A., Rama, B., 2022. IPCC: Climate change 2022: Impacts, Adaptation and Vulnerability. Contribution of Working Group II to the Sixth Assessment Report of the Intergovernmental Panel on Climate Change. Technical Report, Cambridge University Press, Cambridge, UK and New York, NY, USA, p. 3056.

Pugh, D., 1987. Tides, Surges and Mean Sea Level. Wiley and Sons. Chichester, United Kingdom.

Saltelli, A., Annoni, P., Azzini, I., Campolongo, F., Ratto, M., Tarantola, S., 2010. Variance based sensitivity analysis of model output. Design and estimator for the total sensitivity index. Comput. Phys. Comm. 181 (2), 259–270. http://dx.doi.org/10.1016/j.cpc.2009.09.018.

Savage, J.T.S., Pianosi, F., Bates, P., Freer, J., Wagener, T., 2016. Quantifying the importance of spatial resolution and other factors through global sensitivity analysis of a flood inundation model. Water Resour. Res. 52 (11), 9146–9163. http://dx.doi.org/10.1002/2015WR018198.

Seenath, A., 2018. Effects of DEM resolution on Modeling coastal flood vulnerability. Mar. Geodesy 41 (6), 581–604. http://dx.doi.org/10.1080/01490419.2018.1504838.

Seenath, A., Wilson, M., Miller, K., 2016. Hydrodynamic versus GIS modelling for coastal flood vulnerability assessment: Which is better for Guiding Coastal management? Ocean Coast. Manag. 120, 99–109. http://dx.doi.org/10.1016/j.ocecoaman.2015.11.019.

Shaw, J., Kesserwani, G., Neal, J., Bates, P., Sharifian, M.K., 2021. LISFLOOD-FP 8.0: The new discontinuous Galerkin shallow-water solver for multi-core CPUs and GPUs. Geosci. Model Dev. 14 (6), 3577–3602. http://dx.doi.org/10.5194/gmd-14-3577-2021.

Smith, R.A., Bates, P.D., Hayes, C., 2011. Evaluation of a coastal flood inundation model using hard and soft data. Environ. Model. Softw. S1364815211002635. http://dx.doi.org/10.1016/j.envsoft.2011.11.008.

Souto Ceccon, P., Duo, E., Fernandez Montblanc, T., Montes, J., Ciavola, P., Armaroli, C., 2022. A new European coastal storm impact database of resources: The ECFAS effort. In: Proceedings of the 39th IAHR World Congress. International Association for Hydro-Environment Engineering and Research (IAHR), pp. 6646–6652. http://dx.doi.org/10.3850/IAHR-39WC2521711920221117.

Staneva, J., Wahle, K., Koch, W., Behrens, A., Fenoglio-Marc, L., Stanev, E.V., 2016. Coastal flooding: Impact of waves on storm surge during extremes – a case study for the German bight. Nat. Hazards Earth Syst. Sci. 16 (11), 2373–2389. http://dx.doi.org/10.5194/nhess-16-2373-2016.

Stockdon, H.F., Holman, R.A., Howd, P.A., Sallenger, A.H., 2006. Empirical parameterization of setup, swash, and runup. Coast. Eng. 53 (7), 573–588. http://dx.doi.org/10.1016/j.coastaleng.2005.12.005.

Toimil, A., Álvarez-Cuesta, M., Losada, I., 2023. Neglecting the effect of long- and short-term erosion can lead to Spurious Coastal flood risk projections and maladaptation. Coast. Eng. 179, 104248. http://dx.doi.org/10.1016/j.coastaleng.2022.104248.

Toomey, T., Amores, A., Marcos, M., Orfila, A., 2022. Coastal sea levels and wind-waves in the Mediterranean Sea since 1950 from a high-resolution ocean reanalysis. Front. Mar. Sci. 9:991504, http://dx.doi.org/10.3389/fmars.2022.991504.

U.S. Army Corps of Engineers, 2002. Coastal Engineering Manual (Cem). Washington DC, Engineer manual 1110-2-1100.

van de Sande, B., Lansen, J., Hoyng, C., 2012. Sensitivity of coastal flood risk assessments to digital elevation models. Water 4 (3), 568–579. http://dx.doi.org/10.3390/w4030568.

Villanueva, I., Wright, N.G., 2006. Linking Riemann and storage cell models for flood prediction. Proc. Inst. Civ. Eng. - Water Manag. 159 (1), 27–33. http://dx.doi.org/10.1680/wama.2006.159.1.27.

Vinet, F., Lumbroso, D., Defossez, S., 2012. A comparative analysis of the loss of life during two recent floods in France: The sea surge caused by the storm Xynthia and the flash flood in Var. Nat. Hazards 61, 1179–1201. http://dx.doi.org/10.1007/s11069-011-9975-5.

Vousdoukas, M.I., Bouziotas, D., Giardino, A., Bouwer, L.M., Mentaschi, L., Voukouvalas, E., Feyen, L., 2018. Understanding epistemic uncertainty in large-Scale Coastal flood risk assessment for present and future climates. Nat. Hazards Earth Syst. Sci. 18 (8), 2127–2142. http://dx.doi.org/10.5194/nhess-18-2127-2018.

Vousdoukas, M.I., Voukouvalas, E., Mentaschi, L., Dottori, F., Giardino, A., Bouziotas, D., Bianchi, A., Salamon, P., Feyen, L., 2016. Developments in large-Scale Coastal flood hazard mapping. Nat. Hazards Earth Syst. Sci. 16 (8), 1841–1853. http://dx.doi.org/10.5194/nhess-16-1841-2016.

Wagener, T., Pianosi, F., 2019. What has global sensitivity analysis ever done for us? A systematic review to support scientific advancement and to inform policy-making in Earth system modelling. Earth-Sci. Rev. 194, 1–18. http://dx.doi.org/10.1016/j.earscirev.2019.04.006.

Wolff, C., Vafeidis, A.T., Lincke, D., Marasmi, C., Hinkel, J., 2016. Effects of scale and input data on assessing the future impacts of coastal flooding: An application of DIVA for the Emilia-Romagna Coast. Front. Mar. Sci. 3, http://dx.doi.org/10.3389/fmars.2016.00041.